

Department of Mechanical and Aerospace Engineering

**Fatigue Analysis and Comparison of Floating
Offshore Wind Turbine Concepts**

Author: Eliska Sifnerova 201852109

Supervisor: Dr. Erkan Oterkus

Dr. Selda Oterkus

A thesis submitted in partial fulfilment for the requirement of the degree

Master of Science

Sustainable Engineering: Renewable Energy Systems and the Environment

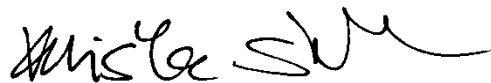
2019

Copyright Declaration

This thesis is the result of the author's original research. It has been composed by the author and has not been previously submitted for examination which has led to the award of a degree.

The copyright of this thesis belongs to the author under the terms of the United Kingdom Copyright Acts as qualified by University of Strathclyde Regulation 3.50. Due acknowledgement must always be made of the use of any material contained in, or derived from, this thesis.

Signed:

A handwritten signature in black ink, appearing to read 'Misha S...' with a stylized flourish at the end.

Date: 23rd August 2019

Abstract

This Master degree thesis presents the research and work done by the author on the problem of fatigue analysis of floating wind turbine concepts. Critical literature review is one of the crucial parts of the work and helps to identify and formulate the research problem in the field. Based on the data and knowledge collected models are formulated. The procedure of the fatigue analysis conducted on those is described and the results are presented. Discussion, conclusions and future work suggestions are included.

Acknowledgments

I would like to thank for the support and valuable advices from all the people involved in the creation of this work. I would like to thank to Dr. Erkan Oterkus and Dr. Selda Oterkus for valuable guidance on the matter of fatigue analysis; to Dr. Maurizio Collu for fruitful discussion regarding the wind turbine concepts for offshore applications; to Dr. Zhiming Yuan for advices on the hydrodynamics of floating bodies.

I would like to thank to Dr. Paul Tuohy for helping resolving administrative issues related to this work and to Mr. Andris Gofmans and to other people involved in prove-reading of this thesis.

Contents

Copyright Declaration 2

Abstract 3

Acknowledgments 4

Contents..... 5

List of Figures 7

List of Tables..... 9

List of Graphs..... 9

Introduction 10

 1.1. Background..... 10

 1.2. About the Problem..... 11

 1.3. Aim of the project..... 12

 1.4. Scope 12

 1.5. Methodology..... 12

2. Literature Review..... 14

 2.1. Offshore Environment 14

 2.2. Offshore Wind Turbines 18

 2.3. Floating support structures and Mooring Systems 25

 2.4. Fatigue Analysis of the FOWT..... 32

 2.5. Modelling Approaches 34

3. Model Description 37

 3.1. Software used 37

3.2.	The Model.....	37
4.	Modelling.....	43
4.1.	Structural and Hydrodynamic modelling	43
4.2.	Coupled Hydro- and Aero-dynamic modelling	45
4.3.	Post-processing.....	48
5.	Results.....	50
5.1.	Three blade HAWT	50
	51
5.2.	Two blade HAWT	57
5.3.	VAWT	59
6.	Discussion.....	60
7.	Conclusions.....	62
7.1.	Conclusions	62
7.2.	Lessons Learnt.....	62
7.3.	Future Work.....	62
8.	References.....	64
	Appendix 1	69
	Appendix 2	70
	Appendix 3	72

List of Figures

Figure 1 - Wind rose for Sevenstones, UK (Cradden et al., 2016) 15

Figure 2 - Weather buoys (National Data Buoy Center, 2008)..... 18

Figure 3 - Average installed WT capacity of offshore installations given year (WindEurope)
..... 18

Figure 4 - Schematic of a HAWT (US Department of Energy)..... 20

Figure 5 - Blade of the Wind Turbine Schematic (Schweigler, 2012)..... 21

Figure 6 - WT power coefficient vs tip speed ratio (Hau, 2013) 22

Figure 7 - The two bladed VAWT layouts..... 23

Figure 8 - Comparison of the HAWT and VAWT concepts (Credit: Josh Paquette and Matt Barone)..... 24

Figure 9 - Floating WT concepts (Jonkman & Buhl, 2007)..... 26

Figure 10 - Semi-sub FOWT (Antonutti et al. 2016)..... 27

Figure 11 - IDEOL's barge supported FOWT (www.ideol-offshore.com) 27

Figure 12 - Spar and the restoring moment..... 29

Figure 13 - Artist's impression of a TLP WT - PetaStar offshore (G. P. Filip) 29

Figure 14 - Slack mooring (Left) and Taut mooring (Right) spread mooring concepts (Ma et al., 2019)..... 30

Figure 15 – Rainflow method performed (top right); hysteresis loop of data (bottom right) (Lee et al., 2012) 33

Figure 16 - GeniE generated mesh and HydroD model 44

Figure 17 - The models of the turbines - (a) three blade HAWT; (b) two blade HAWT; (c) VAWT..... 47

Figure 18 - S-N curve for DNV E grade steel with cathodic protection (DNV)..... 49

Figure 19 - Post-processor layout..... 49

Figure 20 - Displacement of the FOWT depending on the scenario.....	50
Figure 21 - Static position of the two blade HAWT	58
Figure 22 - Two blade HAWT dynamic calculation error message	58
Figure 23 - VAWT task calculation error	59

List of Tables

Table 1 - Standard Roughness Lengths (World Meteorological Organization, 2014).....	16
Table 2 - Wave by source and usual period (based on Munk, 1950).....	17
Table 3 - Sea state definition (based on World Meteorological Organization).....	17
Table 4 - Summary of Advantages and Disadvantages of HAWT and VAWT.....	24
Table 5 – Advantages and Disadvantages of different floating support structure concepts	29
Table 6 - Characteristics of different mooring concepts (González & Diaz-Casas, 2016).....	31
Table 7 - Numerical codes summary table (Robertson et al., 2014).....	36
Table 8 - Environmental Conditions Summary.....	38
Table 9 - Base line WT specifications	39
Table 10 - Properties of the two blade HAWT model	40
Table 11 - VAWT model specifications	42
Table 12 - Lines specifications for two blade HAWT model	46
Table 13 - Lines specifications for the VAWT model	47
Table 14 - Cycles to failure count	57

List of Graphs

Graph 1 - Axial stress history for the Sea State Condition 1	51
Graph 2 - Axial stress history for the Sea State Condition 2	52
Graph 3 - Axial stress history for the Sea State Condition 3	53
Graph 4 - Fatigue Damage Equivalent for Sea State Condition 1.....	54
Graph 5 - Fatigue Damage Equivalent for Sea State Condition 2.....	54
Graph 6 - Fatigue Damage Equivalent for Sea State Condition 3.....	55
Graph 7 - Weighted Fatigue Damage Equivalent for Sea State Condition 1	55
Graph 8 - Weighted Fatigue Damage Equivalent for Sea State Condition 2.....	56
Graph 9 - Weighted Fatigue Damage Equivalent for Sea State Condition 3.....	56

Introduction

1.1. Background

Ever since the industrial revolution the human kind has been releasing harmful CO₂ emissions in large amounts than cannot be absorbed by natural cycles of our planet. These emissions were recognized to cause climate change, which could potentially lead to catastrophic scenarios. (Hansen et. al. 1980) International treaties such as Kyoto Protocol or more recent Paris Agreement imposed limits on greenhouse gasses and target levels for the future. The majority of the developed countries have a climate change strategies implemented through national acts and other governmental policies. Some governments and separate town councils have recently declared a climate emergency (The Climate Mobilization 2019) and mentioned the urge to increase the effort to stop the process. One of the major contributors to the CO₂ emissions production is the energy industry which, however, could be rather easily changed. There are technologies mature enough to help solve the problem; the photovoltaic (PV) panels or the wind turbines (WT), which both are currently economically viable options for certain countries. It is clear enough that the energy from the renewable generation is not dispatchable and it is important to note that there are also other obstacles in the way of 100 % renewable energy production.

Over the years the wind energy industry has progressed substantially. Starting in Scotland, onshore, in the late 19th century, when the WT was for the first time used to generate electricity, with capacity to power several lightbulbs. (Hardy 2010) Nowadays, a standard WT installed on a wind farm is rated in MW. In the 90s' the first steps were taken offshore with bottom fixed commercial windfarms appearing in Denmark. The WT at such sites had rated capacity in kW. The initial movement to offshore generation was due to lack of suitable space onshore. The wind speeds at open sea are generally greater than onshore and in sheltered waters. On average the wind speeds experienced by an offshore WT are about 90 % higher than onshore. (Archer & Jacobson 2005) This is mainly because of the lack of obstacles and almost smooth water surface, mostly only disturbed by waves. With growing WT rated capacity the energy of the higher speed winds can be more efficiently extracted; currently the highest capacity is rated at 9.5 MW (2014 – Vestas offshore WT) and the average rated capacity of newly installed offshore WT in Europe in 2018 was 7 MW (WindEurope 2019).

With higher capacity, the structures are getting bigger, producing more noise, and some may say, are disturbing the views. On the way to low carbon energy the major problem is the cost of integration of the renewables to the current grid as large amount of energy storage would have to be deployed. (Jacobson 2016) One solution could be to spatially diversify the wind farms to manage the variability of the resource. (Santos-Alamillos et. al. 2014) In Europe this encourages the industry to go further offshore, where the water depths are increasing (>50m) and the fixed offshore wind turbine concept is no longer economically feasible and structurally viable, therefore floating offshore wind turbine (FOWT) concepts have to be adapted. For other countries involved in research and development (R&D) of floating wind concepts, the background drive may be different. Europe is lucky with its relatively shallow waters of the North Sea, but countries such as Japan or the USA cannot profit from such benefits as their coastal waters are going deep rather steeply.

The WT are designed for 20 years of operational life with preferably as little maintenance as possible. Through the lifetime the WTs are exposed to continuous dynamic loading from wind and its floating support and mooring to loads induced by waves, currents and tides. The repeated loading causing change in stresses in the structure leads to fatigue damage which can ultimately lead to failure of the structure. This phenomenon needs to be accounted for and therefore a fatigue analysis (FA) needs to be performed.

1.2. About the Problem

The FA in wind energy industry has become a common practice. The main concern of the FOWT is the design and selection of the floater. Only very little attention is paid to different turbine concepts. At the current state of the art of the FOWT only the best concept derived for onshore – the 3 bladed horizontal axis wind turbine HAWT is considered for the ongoing demonstration projects. This is a trend supported by the current industry standards, such as IEC 61400-3-2 where the development of the WT for offshore floating applications based on the general IEC 61400-1 which prescribes the land based WT design. There is only a little attention in the research community and almost no interest from the industry, on what is the best option for the FOWT. Some researchers point out the better scalability, aerodynamic performance and structural behaviour of a vertical axis wind turbines VAWT; others highlights the possibility of usage of the high-speed rotation downwind 2-bladed HAWT with possibly better performance in higher wind speeds than the 3-bladed HAWT.

1.3. Aim of the project

The robustness of FA for 3-bladed HAWT offshore concepts is doubtless; however, very little effort was made to conduct FA for 2-bladed HWAT and VAWT offshore concepts and compare the structural behaviour of the three. This thesis will conduct fatigue analysis and then a comparison study of the three different turbine concepts of the same rated capacity mounted on a SPAR buoy at the same location.

1.4. Scope

This study was conducted to determine which of the three concepts is the structurally best performing in terms of fatigue loading and structural properties in the same environmental conditions.

1.5. Methodology

The work is structured into following chapters; each chapter corresponds to one step in the methodology of the project:

- Chapter 2: Critical Literature Review

The literature review was focused mostly on work done on design and fatigue analysis of FOWT. International design standards were developed as well as guidelines for loads consideration as. The work on different FOWT concepts included studies on comparison of floater options, but very little was done on the matter of different turbines mounted on the floater. Literature on fatigue analysis in general was reviewed for reference. A brief introduction to wind resource and modelling techniques suitable for WT is included in this chapter.

- Chapter 3: Model Description

Based on the literature reviewed in chapter 1, the basic components for the models were identified and selected. Several scenarios will be modelled. The model will have a floating Phase IV OC3 SPAR support, with catenary mooring and will be mounted with a 5 MW NREL reference offshore WT. The baseline scenario will contain wind and wave environmental forces. Two further scenarios will be explored; these will contain current: in the first case the current and the wind are in the same direction, whereas in the second case the current will be opposite to the wind direction. If the time will allow, two further turbine options will be considered for the same environmental conditions as in the three initial scenarios – the turbines will be a 5MW VAWT and 5MW two blade downwind HAWT.

- Chapter 4: Modelling

This chapter will describe the procedure taken to model all the scenarios, including the design of the floating SPAR and the different WT types, pre-processing and environment modelling. Additionally, the selected softwares and basic principals used by the softwares will be enclosed in this chapter.

- Chapter 5: Results

Results of all modelled scenarios will be presented in this section. The results will be presented in the form of graphs representing each of the three modelled sea state conditions, Fatigue Damage and Weighted Fatigue Damage as well as the Accumulated Damage. Additional data such as scenario-dependent displacement of the FOWT will also be present.

- Chapter 6: Discussion

A discussion on the results of the work will be presented, a reflection on lessons taken from this work will be provided and a recommendation for future work will be included in this chapter.

- Chapter 7: Conclusions

In this chapter the summary and the results of the work will be presented, accompanied by the conclusions and the lessons learnt. Future developments of the work will be also proposed in this section.

2. Literature Review

As part of this study a critical literature review was carefully conducted. There was a substantial amount of work done in the field of offshore wind energy production. The work was mainly concentrated on studies of the bottom fixed turbines and due to the recent developments and needs the focus shifted to the FOWT.

This chapter covers the theoretical part and research conducted before starting the practical modelling. A brief introduction to the wind resource and wind characteristics is offered. The WT's and floating supports comparison is conducted in this chapter as well as the basics of physics governing the FOWT problems and modelling methods are explained further.

2.1. Offshore Environment

In the wind energy industry it was always crucial to know the strength of the wind in the area of interest. The floating offshore wind industry, however, has to consider other environmental aspects alongside with the wind. The wave and typical sea condition are another important to account for in case of the floating structures. Other conditions such as currents and ice are important for design too but will not be discussed in the literature review; in case of further interest the reader is referred to Cradden et al. (2016).

2.1.1. Wind Resource

The first important step in the wind energy extraction is the assessment of the wind resource. As it will be shown in equation 1, the energy content varies with the wind speed (u) cubed. The theoretical wind power (P_t) can be calculated as wind energy per unit time as follows:

$$P_t = \frac{1}{2} \rho A u^3 \quad (1)$$

Where the A is the rotor's swept area, ρ is the air density and u is the wind speed.

In order to be able to assess the potential, it is important to understand what a wind is (Salameh, 2014). There are different scales of wind, ranging from global to local scale wind. The wind is a movement of air caused by pressure differences in the atmosphere. The air is displaced from high pressure zones to the zones with lower atmospheric pressure. This pressure difference is caused by uneven heating of the Earth surface. There are different scales of wind starting with global steady winds high in the atmosphere, which are periodic and highly predictable; ending with local wind which changes as quickly as weather can change.

Wind measuring is happening for a long time in human history, wind maps exist and are a representation of the wind speed in the given area. The wind measuring on shore has a long

tradition, offshore not so much. The measuring of the local wind offshore is conducted by several different means. The network of measuring “stations” (e.g. meteorological buoys, oil & gas platforms) is sparser than on shore, which makes creating long term data sets for development of offshore windfarms difficult. It is important to assess not only the wind speed but also the direction of the wind. To represent the collected data on a local level wind roses are used. The wind roses are capable of representing the direction and wind speed in one plot. An example of a wind rose can be seen in [Figure 1](#)– this wind rose is the representation of the wind resource at the Sevenstones.

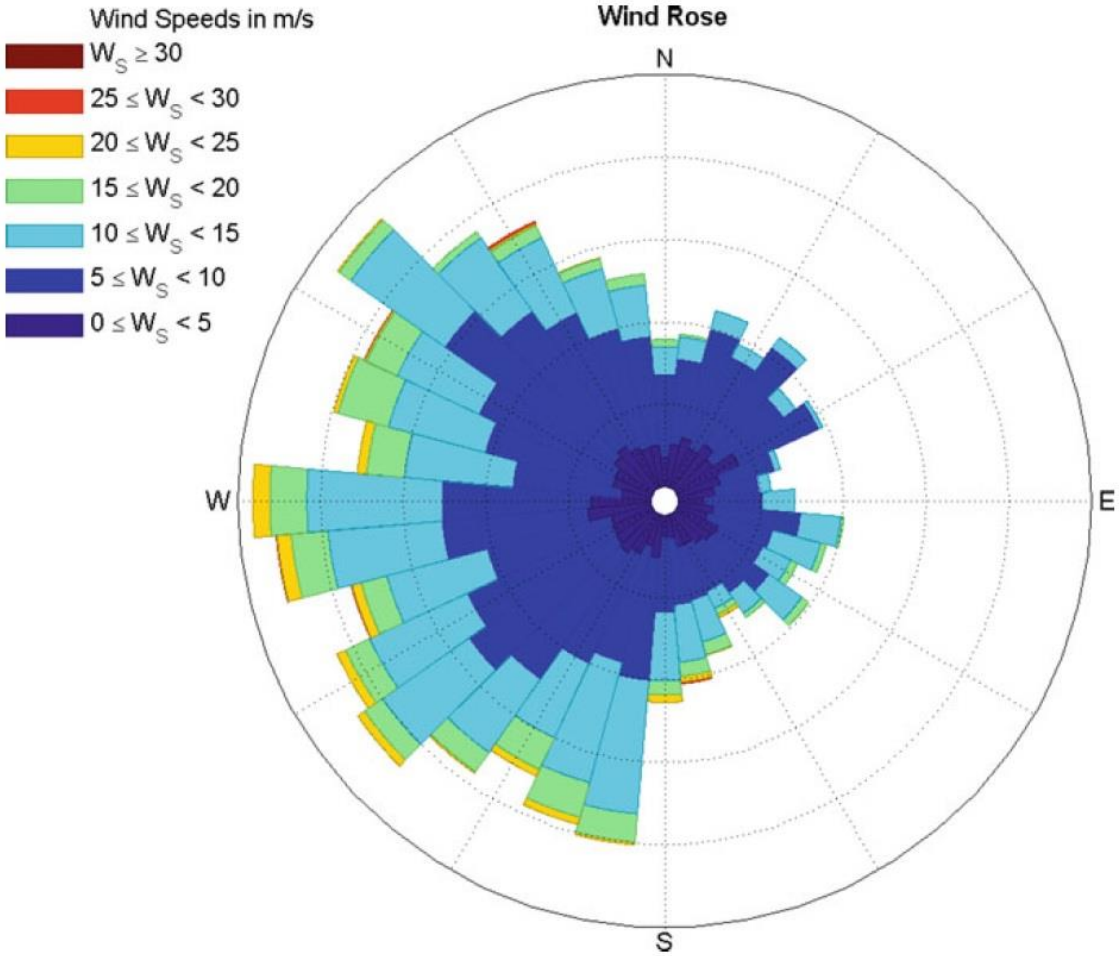


Figure 1 - Wind rose for Sevenstones, UK (Cradden et al., 2016)

As one can note the winds offshore are on average stronger than on shore. This is due to the fact, that there are more obstacles for wind flow on shore than offshore. In the wind speed calculations this is represented by a roughness length (z_0). The flatter the surface and surroundings is, the lower the roughness is. Offshore there are very little structures obstructing the wind and the only unevenness of the surface are the waves. This leads to assumed roughness length for offshore calculations to be $z_0=0.0002$ m, comparing this value to a roughness length for flat grassland $z_0=0.03$ m leads to great wind speed differences based

on the equation (2). The local wind speed (u) at a given height above the ground (z) can be calculated as:

$$u = U_{ref} \frac{\ln \frac{z}{z_0}}{\ln \frac{z_{ref}}{z_0}} \quad (2)$$

Where U_{ref} is the reference wind speed at reference height above the ground level z_{ref} and z_0 is the surface roughness. Standard surface roughness lengths established by the World Meteorological Organization (WMO) are listed in the [Table 1](#).

Table 1 - Standard Roughness Lengths (World Meteorological Organization, 2014)

Terrain description	z_0 (m)
Open sea, fetch at least 5 km	0.0002
Mud flats, snow; no vegetation, no obstacles	0.005
Open flat terrain; grass, few isolated obstacles	0.03
Low crops; occasional large obstacles, $x/H > 20$	0.10
High crops; scattered obstacles, $15 < x/H < 20$	0.25
Parkland, bushes; numerous obstacles, $x/H \approx 10$	0.5
Regular large obstacle coverage (suburb, forest)	1.0
City centre with high- and low-rise buildings	≥ 2

2.1.2. Wave Climate

Munk (1950) has categorized waves by their period and the driving phenomenon. The most common waves are short period waves caused by wind. These waves are the usual waves observed daily on the sea. Other daily repeating waves are caused by the positioning of the sun and moon and are known as tidal waves. The complete categorization and details are depicted in Table 2. Other common description of a sea condition is a sea state. This categorization is more useful for the modelling purposes as each sea state can be represented by an energy spectrum which contains information about the wave height and the wave period. The sea state categorization by the World Meteorological Organization is presented in [Table 3](#).

Just like the wind, the sea states and wave energy density vary through the year. During the winter period of the region in question it is common to observe on average higher sea states than in summer period.

The IEC 64100-3-2 is highlighting the fact that the highest wind speeds and highest waves do not usually appear together, and therefore it is in accordance with the standard to use lower wind speeds for high sea state load estimations.

Table 2 - Wave by source and usual period (based on Munk, 1950)

Classification	Period	Source
Trans-tidal waves	24 h and up	Storms, sun and moon
Ordinary tides	12–24 h	Sun and moon
Long-period waves	From 5 min to 12 h	Storm and earthquakes
Infra-gravity waves	From 30 s to 5 min	Wind
Ordinary gravity waves	From 1 to 30 s	
Ultra-gravity waves	From 0.1 to 1 s	
Capillary waves	Less than 0.1 s	

Table 3 - Sea state definition (based on World Meteorological Organization)

Sea State	Wave Height	Description
0	0 m	Calm (glassy)
1	0 – 0.1 m	Calm (rippled)
2	0.1 – 0.5 m	Smooth (wavelets)
3	0.5 – 1.25 m	Slight
4	1.25 – 2.5 m	Moderate
5	2.5 – 4 m	Rough
6	4 – 6 m	Very rough
7	6 – 9 m	High
8	9 – 14 m	Very High
9	Over 14m	Phenomenal

The data collection of wave characteristics of a region is difficult. Nowadays, it is collected by the meteorological buoys. The downside is the maintenance of such devices. In the [Figure 2](#) the diverse weather buoys used by US National Data Buoy Centre are represented. The size of the buoy usually depends on the equipment installed, water depth of the installation and the type of the buoy. The drifting buoys are smaller than the moored buoys.

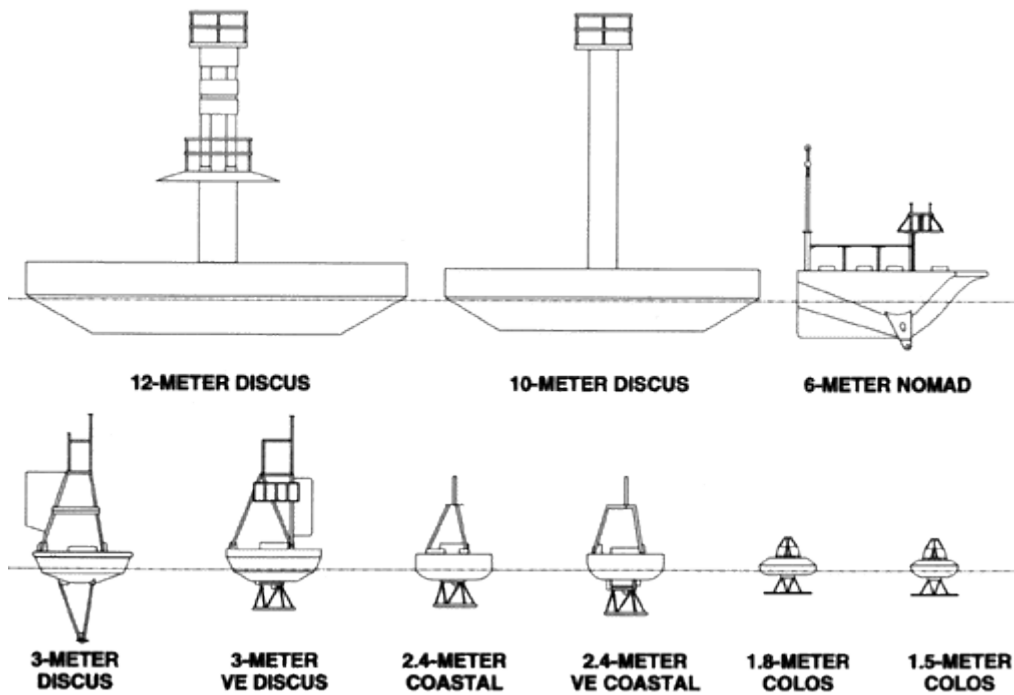
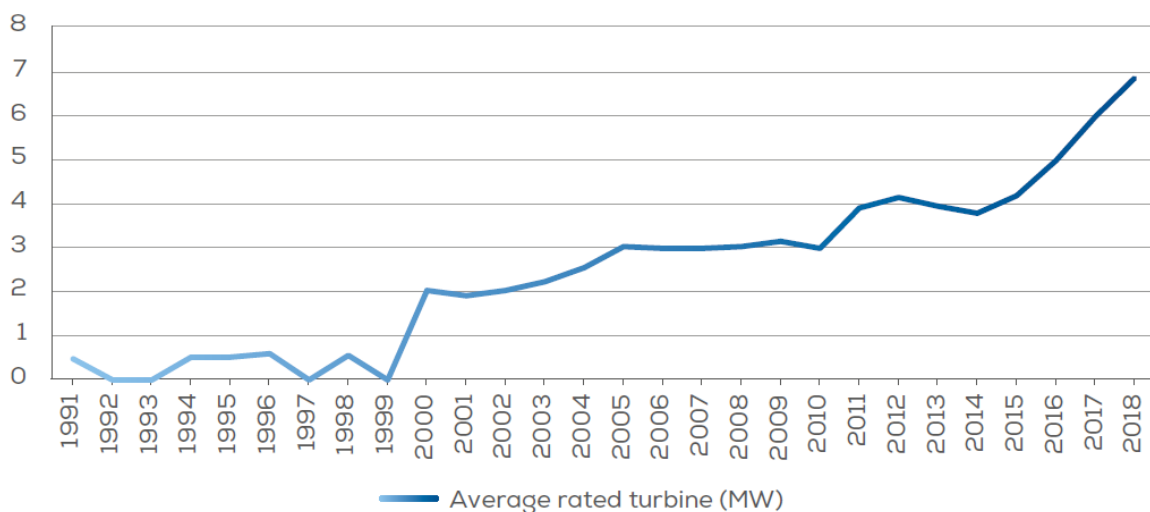


Figure 2 - Weather buoys (National Data Buoy Center, 2008)

2.2. Offshore Wind Turbines

As the wind turbines are getting bigger there is a need to go deeper offshore as bigger machines require more space, stronger wind resource and are a concern of visual and noise impact (Ma et al., 2014). The wind resource is stronger offshore due to the low surface roughness compared to onshore (Neill et al., 2018) The average installed offshore WT rated capacity growth is in [Figure 3](#), where the growing rated capacity trend in past 20 years is clearly visible and it can be demonstrated, that large multi-mega-watt turbines are not only a matter of R&D.



Source: WindEurope

Figure 3 - Average installed WT capacity of offshore installations given year (WindEurope)

There are two different types of wind turbines – the horizontal axis wind turbine (HAWT) and the vertical axis wind turbine (VAWT). At the very beginning of the modern wind energy industry both of the concepts were investigated. Due to the fatigue loads on the blades of the Darrieus turbine and the blades manufacturing complexity, the HAWT has been established as the basic concept for commercial use onshore. The HAWT was adapted to fixed offshore use and now expanded on the floating supports. Henderson et al. (2016) in the entry to the “Floating Offshore Wind Energy – The Next Generation of Wind Energy” compares the two concepts with relation to the floating wind energy extraction. According to Borg et al. (2014) adapting the VAWT concept for FOWT could be beneficial as this concept provides better aerodynamic properties suitable for offshore floating installations than HAWT. The following sections give a comparison of the two concepts. It is worth mentioning that investigations into multi-turbine platforms and novel kite power extraction devices are under research. A summary of advantages and disadvantages of the concepts are in the [Table 4](#) at the end for the section.

2.2.1. Horizontal Axis Wind Turbine

The HAWT turbines can be further divided into two categories based on the direction of the wind passing through the turbine – upwind turbines and downwind turbines, of which the first is more common. Lately Japan is investing in conducting further research of testing for the downwind variation. The widely used HAWT is composed from the following parts: a tower, a nacelle, a rotor (hub) with blades. The tower supports the nacelle and rotor with blades. The nacelle is a house to the gearbox, generator, brakes and low- and high-speed shafts. At the front of the nacelle a rotor with blades is placed. The [Figure 4](#) depicts closely the usual system layout. A list of the components and their functions is provided based on Neill & Hashemi (2018): Anemometer, Blades, Brake, Controller, Gear Box, Generator, High-speed shaft, Low-speed shaft, Nacelle, Pitch system, Rotor, Tower, Yaw drive, Yaw motor.

- *Anemometer* – a wind measuring device, the data collected is sent to the system to eventually stop the WT if the wind speed is too high;
- *Blades* – are attached to the rotor which spins as the wind applies force on the blades; blades are large air foils usually made from composite materials;
- *Brake* – stops the rotor in times of emergency/high wind speeds;
- *Controller* – system turning on and switching off the turbine;

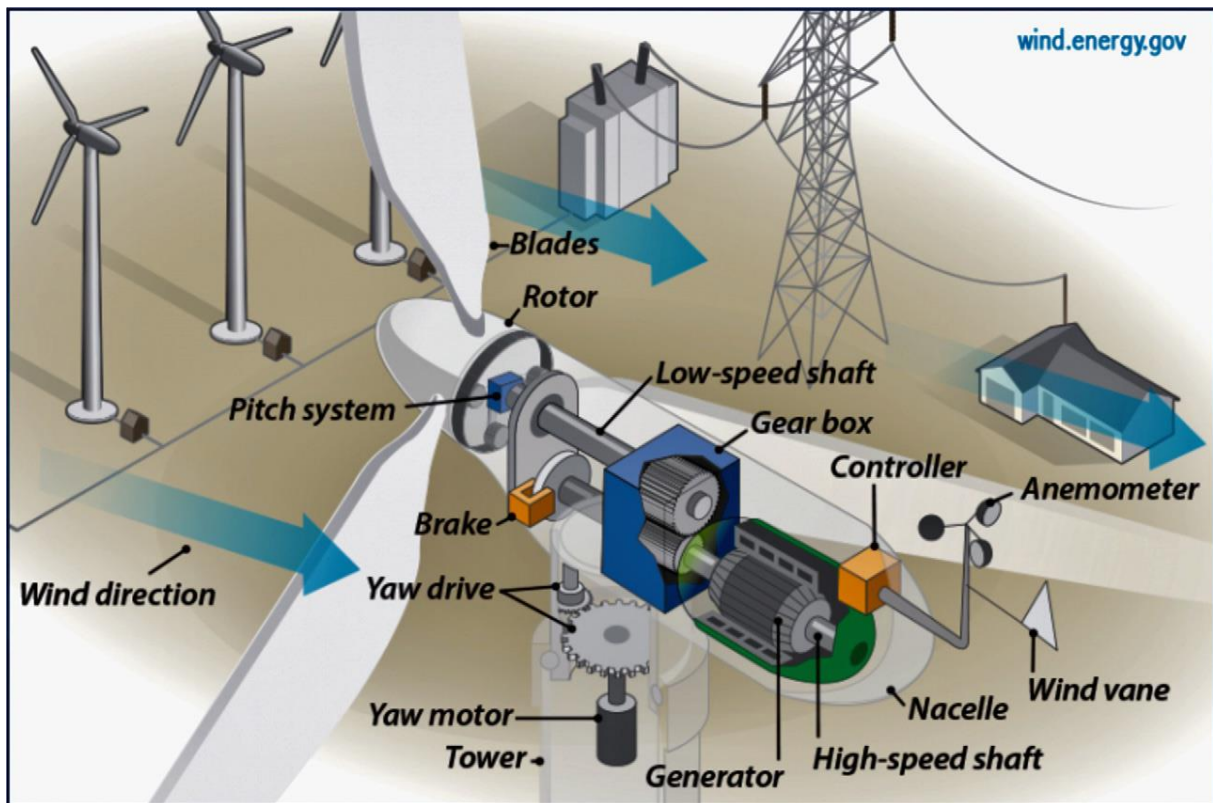


Figure 4 - Schematic of a HAWT (US Department of Energy)

- *Gear Box* – transfers the torque produced by the rotor from the low-speed shaft to the high-speed shaft end to the generator;
- *Generator* – produces electricity;
- *High-speed shaft* – drives the generator, transmits the power from the gear box;
- *Low-speed shaft* – transfers the torque generated by the rotor to the gear box;
- *Nacelle* – all the WT instrumentations is housed in there;
- *Pitch system* – turns the blades to adjust the angle of attack for maximum energy extraction;
- *Rotor* – omnibus name for blades and hub
- *Tower* – supports the WT
- *Yaw drive* – aligns an upwind WT to the wind direction
- *Yaw motor* – powers the yaw drive

The power extraction by a WT is possible due to the blades and its properties. A general shape of the blade is like an airplane wing. The side of a leading edge with a bigger curve has lower pressure compared to the other side in the air flow. This will cause lift being generated on the blade and makes it spin the rotor. A blade description can be observed in [Figure 5](#).

It is important to point out that the twist of the blade end improves the performance of the rotor. Comparing the linear velocities of the blade tip and the rotor will lead to an observation of tip velocity is much higher than the rotor's velocity. The twist helps to maintain same angle of attack and thus improves the WT efficiency. (Burton et al., 2011) Some of the WTs have blades with a precone. This is an end part of the blade which is pre-bend to improve the aerodynamics.

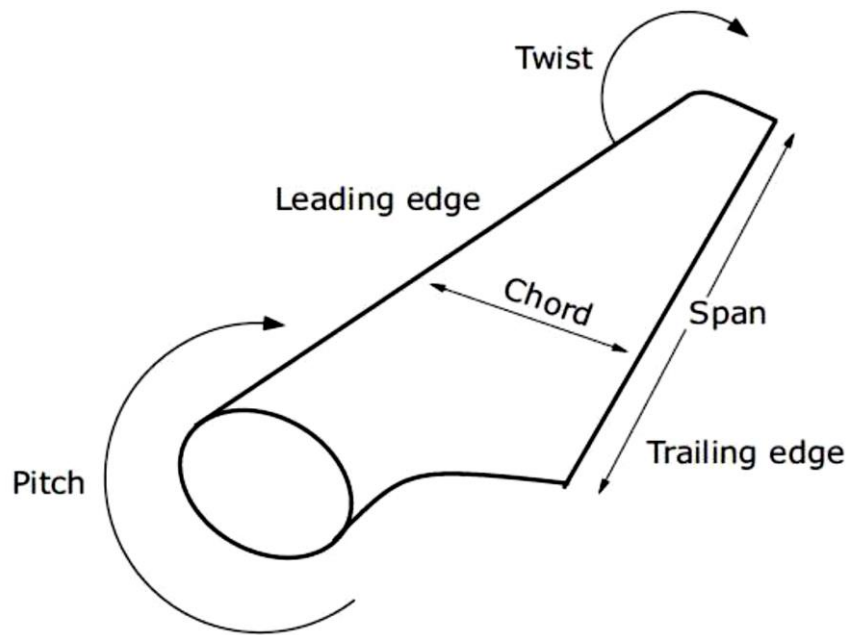


Figure 5 - Blade of the Wind Turbine Schematic (Schweigler, 2012)

Different number of blades can be found on the rotor, from the engineering and cost effective point of view a three-bladed variant is the most suitable. Turbines with even number of blades tend to suffer from larger bending moments at the bottom of the tower when the lower blade passes by the tower and the upper blade gets the most energy from the wind and bends. Both one- and two-bladed WT exist on the market but are not as highly considered as the 3-bladed variant, due to problems which are hard to solve on onshore installations. These variations need higher wind speeds to produce the same rated output, therefore the rotation speeds and noise pollution is higher (Salameh, 2014). The [Figure 6](#) presents a graph of different types of rotors, their respective power coefficients vs the tip speed ratio. The power coefficient (c_p) is defined as the extracted power (P_e) (generated electricity) over the available (theoretical) wind power (P_t):

$$c_p = \frac{P_e}{P_t} \quad (3)$$

The maximum theoretical c_p can be 0.593, called the Betz law (limit) and is obeyed by all WT (Neill & Hashemi, 2018).

The larger bending moments exerted on the tower can be lowered potentially by a floating support as this allows the tower to tilt instead of purely bent as in the fixed cases. The two and one blade WT also offers a weight reduction of the top of the tower, which is beneficial for FOWT. The two blade WTs for FOWT are currently under development and tested in Japan. According to Henderson et al. (2016) it should be noted that there is a limit to up-scaling the HAWTs without implementing not yet developed novel technologies. The economical limit is stated between 15 to 20 MW for a single turbine.

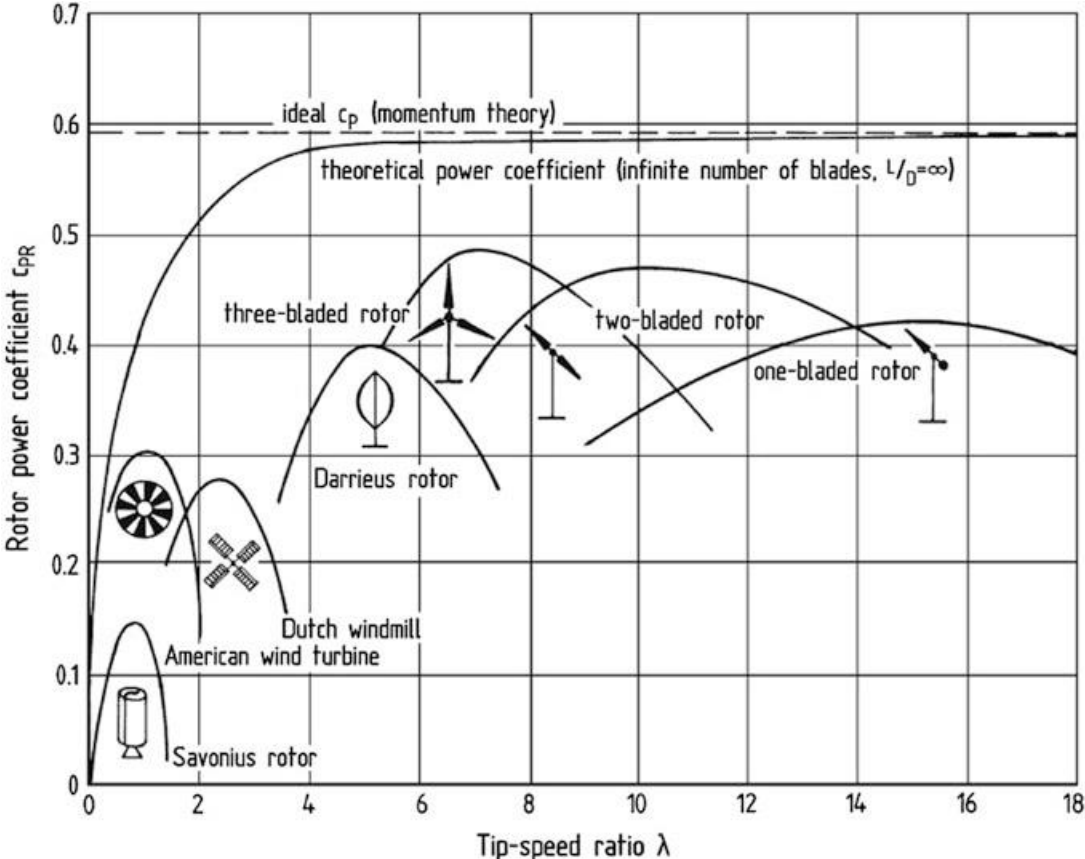


Figure 6 - WT power coefficient vs tip speed ratio (Hau, 2013)

2.2.2. Vertical Axis Wind Turbine

There are different layouts of the VAWT concepts, according to various studies a two blade VAWT is the most suitable for the marine applications (Hand & Cashman 2017; Borg et al. 2014). Within the two blade concept pool there are several categories – the Ω rotor, the H rotor and a V rotor. The three different layouts are compared in the Figure 7 for better reference. The Ω rotor or the Darrieus rotor (Figure 7a) has two blades closed into one big loop, the problem with this concept is the difficulty of the blade fabrication and the fatigue damage the blades are exposed to. The H rotor (Figure 7b) has two blades attached to the tower by struts (one or two per blade). The issue with H rotor is the presence of the undesirable added resistance of the rotor caused by the attached struts. Hand & Cashman

(2017) have proposed H rotor as the ideal concept for FOWT. The concept had two aerodynamically improved struts per blade for lower resistance. The advantage of this concept is the simplicity of the blades, which then are easy to manufacture in series. The V rotor (Figure 7c) was presented by the Borg et al. (2014) using the bottom half of the Darrieus rotor, showing promising results in terms of aerodynamics and fatigue of the blades.

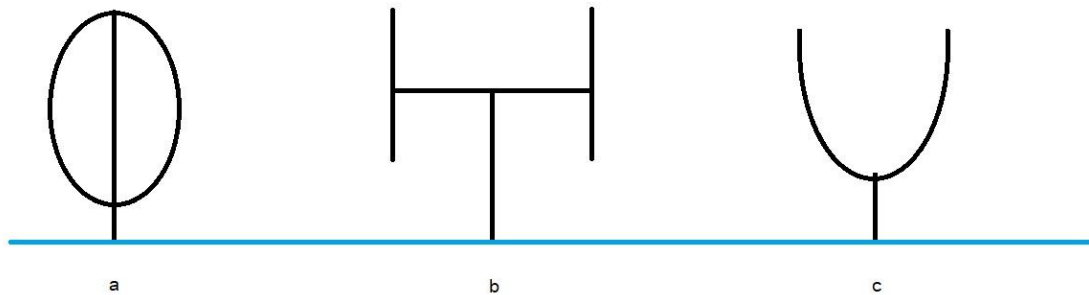


Figure 7 - The two bladed VAWT layouts

Borg et al. (2014) has conducted through research in the field of the floating vertical turbines with his team. The aim was to develop a modelling tool for the floating VAWTs. Prior to that an extensive research on the VAWTs in the offshore environment was conducted and presented in three separate issues addressing the aerodynamics (2014), mooring and structural dynamics (2014) and hydrodynamics (2015). In the Part I: Aerodynamics (2014); VAWT's better suitability for floating supports has been mentioned. This is given by the VAWT's performance being less affected by the rotational motions induced by the environmental forces, especially when heeled backwards by the wind passing through the turbine. Whittlesey et al. (2010) have demonstrated that the VAWT's wake dissipates faster compared to the HAWT's wake. Even though there is no space problem offshore (yet), this fact could significantly save on the length of the export cables and therefore save finances. A VAWT comprises of: rotor with blades (usually 2 for offshore applications), shafts and generator and a controlling mechanism with brakes and wind measuring devices all of which have the same function as described in the paragraph 2.2.1. When comparing the HAWT and VAWT it is important to note where the mass is concentrated. In the case of the HAWT the nacelle with all the instrumentation is located on the top of the tower. This is not the case for the VAWT. The instrumentation of the VAWT can be located at the bottom of the tower close to the water surface or even in the floater, which makes the access for maintenance easier, as well as the tower in case of scaling up the turbine will not suffer from vast bending moments as in the case of HAWT (Henderson et al., 2016), which for large scale turbines (above 15MW) proves economical. A Figure 8 depicts the different layout of the two concepts. It is also important to

mention the simplicity of the VAWT concept compared to the HAWT concept. The VAWT does not need complex controllers for blade pitch nor yaw systems as the direction of the wind is not important for the VAWT.

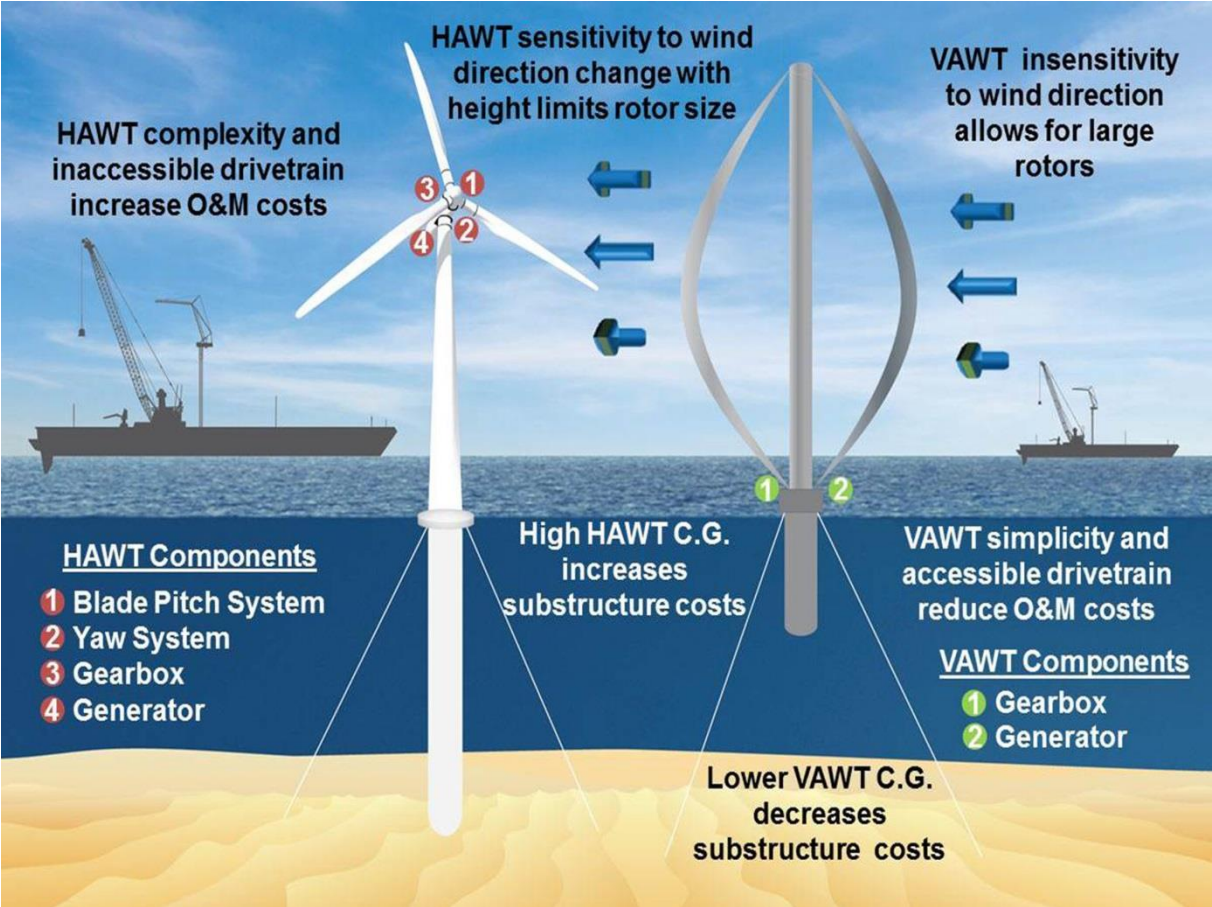


Figure 8 - Comparison of the HAWT and VAWT concepts (Credit: Josh Paquette and Matt Barone)

The same Betz limit and power coefficient according to equation (3) applies for VAWT as for HAWT, and researchers argue that the HAWT design has better performance than the VAWT. This is true until high-speed winds are accounted for. The usual cut-out wind speed for a HAWT is around 25m/s; on the other hand the cut-out wind speed for VAWT could be as high as 65m/s (Islam et al., 2013).

Table 4 - Summary of Advantages and Disadvantages of HAWT and VAWT

Type	Advantages	Disadvantages
HAWT	<ul style="list-style-type: none"> • Mature concept • Higher reliability • Higher efficiency 	<ul style="list-style-type: none"> • Mass concentrated on the top of the tower • Difficult maintenance

Table 4 continued - Summary of Advantages and Disadvantages of HAWT and VAWT

Type	Advantages	Disadvantages
HAWT		<ul style="list-style-type: none"> • High sensitivity to tilt angle • Higher sensitivity to wave induced motions
VAWT	<ul style="list-style-type: none"> • Insensitivity to wind direction • Easy access to the instrumentation • Potential for smaller floater for the same rated power <p>Superior aerodynamics in higher wind speeds</p>	<ul style="list-style-type: none"> • Optimal design was not reached yet • R&D stage <p>Difficult fabrication of the blades (especially Darreirus rotor)</p>

2.3. Floating support structures and Mooring Systems

The suitable space for bottom fixed offshore WT in shallow waters is not infinite and in depths larger than 50 m the fixed concept is not economically viable option. The supporting structures of floating offshore wind turbines (FOWT) are inspired by the offshore oil and gas industry. There are three main floating concepts use for the oil and gas exploration and extraction; each of these concepts use different principal to keep stability as well as each provides a different set of benefits and set-backs. The semi-submersible platform relies on hydrostatics and sufficient distributed buoyancy of the body. The SPAR concept keeps its stability thanks to major ballast placed at the bottom of its cylindrical structure, and the tension leg platform (TLP) is stable due to the tension of its tendons. The concepts are illustrated in Figure 9. The semi-sub and SPAR buoy concepts are kept in station by slack mooring lines.

The offshore wind community recognizes that each site needs a different solution. The Energy Technologies Institute recommends TLP as the most suitable design for the UK waters. It may be noted that the industry had a different opinion and in 2017 the first commercial floating wind farm was commissioned off the Scotland's coast supported by SPAR buoys. The pros

and cons of the three concepts will be discussed in the following sub-sections of this chapter and are summarised in Table 5 at the end of section.

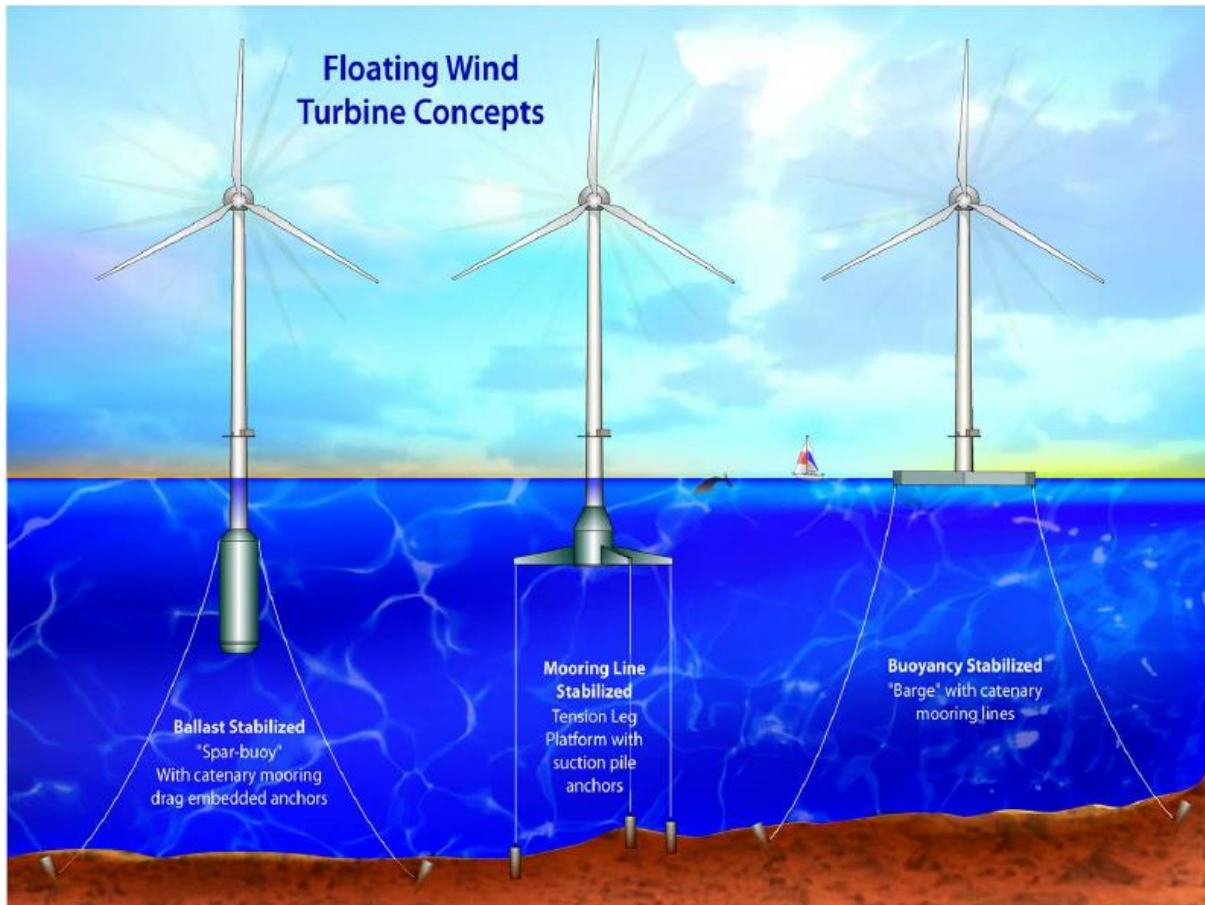


Figure 9 - Floating WT concepts (Jonkman & Buhl, 2007)

2.3.1. Semi-Submersible supports and Barges

The concepts rely on buoyancy as its main means of stability. The concepts are fully stable without mooring lines. A semi-sub usually consists of three to four main columns providing sufficient buoyancy, which are connected by a lattice structure. For illustration, the semi-submersible can be observed in [Figure 10](#). A barge is usually a rectangular structure with a moon pool (damping pool) opening in the centre to improve the hydrodynamic responses of the structure. The moon pool can be observed in [Figure 11](#). The structures suffer of large water-plane areas which makes seakeeping in high sea states difficult to manage. The high responses in roll, pitch and heave can be observed and it is important in the design stage to make sure the natural frequency of the platform in these motions are as far as possible from the wave frequency of the development site. (Henderson et al., 2016) To reduce the heave motion, heave plates are installed on the bottom of the floating structure. The WT usually sits either in the centre or on one of the columns in case of the semi-sub or in the centre of one of the sides of the barge ([Figure 11](#)). Recent developments in the barge type support have led to

demonstration projects in Japan and in France. As of July 2019, there is an approved project for a commercial size windfarm in Japan with barge type floater (www.odeol-offshore.com). Slack mooring systems are used for station keeping of the platform, discussed in [2.3.4](#).

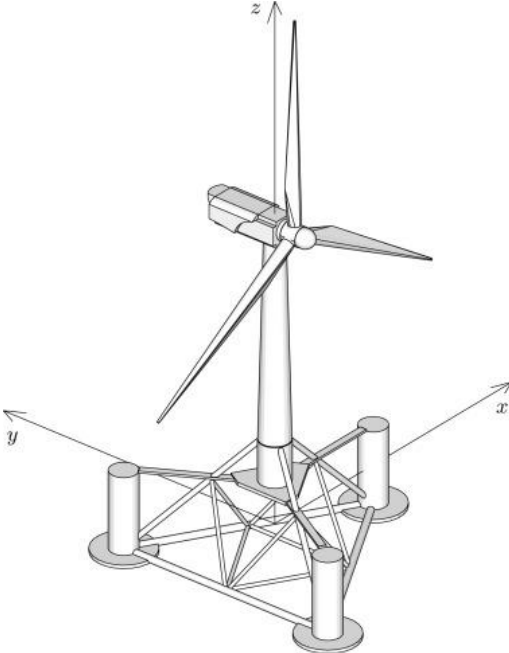


Figure 10 - Semi-sub FOWT (Antonutti et al. 2016)



Figure 11 - IDEOL's barge supported FOWT (www.ideal-offshore.com)

2.3.2. SPAR buoy supports

The Spar buoys are ballast stabilized platforms. The floater is stable without mooring as the centre of gravity is well lower than the centre of buoyancy to keep the structure upright due to the ballasting weight (usually water/gravel/concrete) at the bottom (Figure 12). The long cylindrical slender structure attached to the seabed by slack mooring. A disadvantage might be its length as the draught of the buoy is usually close to 100m. This limits the concept application to deep waters in the offshore wind context. A question about sub-stations for such locations should be raised. It is common to have fixed support substations, which may not be applicable in the case of the spar buoy supported structure. Ideol recently introduced a first floating sub-station concept. (www.ideol-offshore.com) On the other hand the large draught improves the structure's behaviour in the heave motion as the water-plane area is generally small and wave elevation forces act only close to the water surface. With a WT mounted on the top, larger bending moments are expected due to the overall height of the structure. (Henderson et al., 2016)

2.3.3. TLP supports

A tension leg platform relies on the stability provided by its mooring. The lines are designed to be axially rigid which makes the TLP to have lower amplitudes in heave, roll and pitch motions. This makes the concept the most stable option amongst the other floating possibilities when fully installed. The concept is depicted in the Figure 13. The platform motions in surge, sway and yaw are present. Since the lines are designed not to elongate, this makes the platform to submerge deeper when in the mentioned motions. This response is called "set-down". It is critical for systems with three or four lines not to lose any as this would likely result into a complete loss of the structure, because as mentioned above the platform is inherently instable without the mooring. This type of platform is suitable only for certain locations as the taut mooring has certain specifications on soil and other environmental conditions as discussed further in section [2.3.4](#). This platform concept has small water-plane area which benefits its seakeeping properties. The installation of the concept is costly compared to the other options due to the more technically challenging tensioned line installation (Handerson et al., 2016).

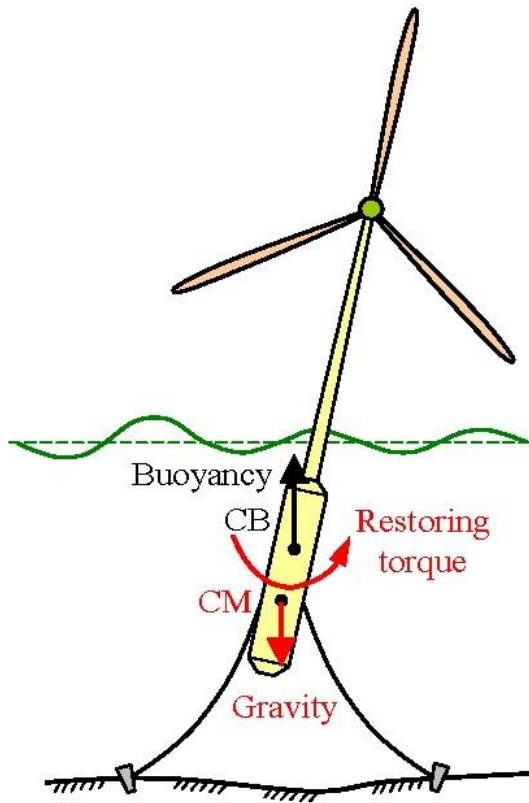


Figure 12 - Spar and the restoring moment (Dihn & Basu, 2013)

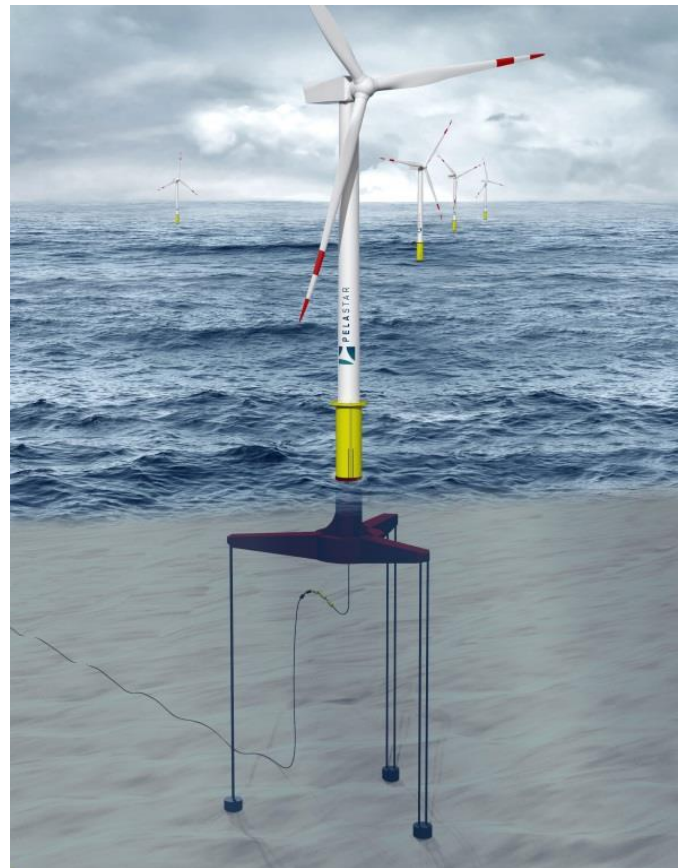


Figure 13 - Artist's impression of a TLP WT - PetaStar offshore (G. P. Filip)

Table 5 – Advantages and Disadvantages of different floating support structure concepts (González & Diaz-Casas, 2016)

Type	Advantages	Disadvantages
Spar buoy—ballast stabilized	<ul style="list-style-type: none"> • Simple design is amenable to serial fabrication processes • Few moving parts (no active ballast required) • Excellent stability 	<ul style="list-style-type: none"> • Constrained to deep water locations • Offshore turbine assembly requires dynamic positioning vessels and heavy-lift cranes • Large draft limits ability to tow the structure back to port for major repairs
Tension leg platform (TLP)—mooring line stabilized	<ul style="list-style-type: none"> • Low structural mass • Onshore turbine assembly • Few moving parts (no active ballast required) • Excellent stability 	<ul style="list-style-type: none"> • High loads on the mooring and anchoring system • Challenging installation process • Bespoke installation barge often required
Semi-submersible platform—buoyancy stabilized	<ul style="list-style-type: none"> • Flexible application due to the ability to operate in shallow water depths • Low vessel requirement—only basic tug boats required • Onshore turbine assembly • Amenable to port-side major repairs 	<ul style="list-style-type: none"> • High structural mass to provide sufficient buoyancy and stability • Complex steel structures with many welded joints can be difficult to fabricate • Potentially costly active ballast systems

2.3.4. Mooring Systems

Essentially, there are two types of mooring that can be encountered in the FOWT industry – slack (catenary) mooring or taut/tensioned mooring (Figure 14). Catenary mooring is based on the traditional ship anchoring systems. The lines are longer than in the latter case and the footprint on the seabed is bigger as part of the lines is lying directly on the seabed. (Ma et al., 2019) The material usually used for the catenary mooring is either steel chains or for deeper water applications it might be polymer rope chains with neutral buoyancy and clumped weights (Henderson et al., 2016). The taut (tension) legs have smaller footprint on the seabed as only the anchoring system is touching it. The tension legs are made from high modulus polymer materials (polyester or polyethylene). The taut concepts are more economically viable for water depths larger than 200m. This is due its shorter length and the cost of the materials compared to the steel chains. A hybrid semi-taut mooring exists, this kind of mooring has its lower leg part catenary which is then connected to the vessel by a taut line.

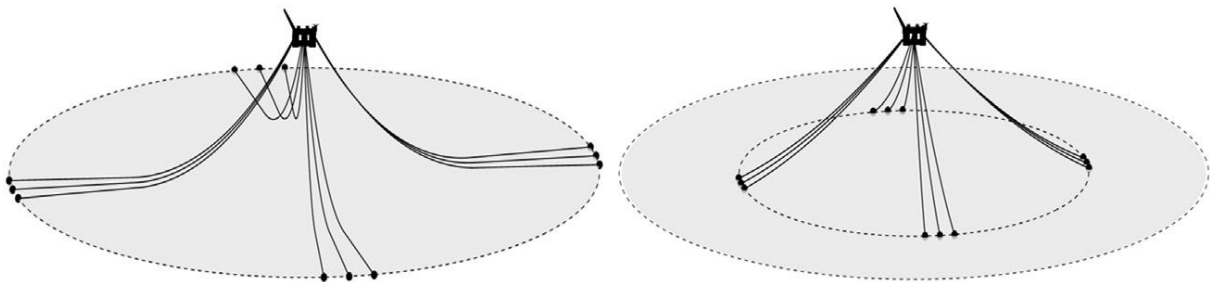


Figure 14 - Slack mooring (Left) and Taut mooring (Right) spread mooring concepts (Ma et al., 2019)

Three different configurations of mooring are used within the industry – spread mooring, tension leg system (TLP, TLS) and a single point mooring. The spread mooring is depicted in the Figure 14 above. This system is attached to various points around the hull of the structure restricting the surge, sway and yaw motions of the structure (Ma et al., 2019). The TPS limits the heave motions of the platform while leaving surge, sway and yaw motions compliant (Handerson et al., 2016). The TPS are limited to larger water depths and suitable seabed materials due to the specific anchoring systems. In the single point mooring systems, the mooring lines are attached to the centre of rotation and the platform is free to yaw. Principal characteristics of a taut, semi-taut and catenary mooring are given in Table 6.

The mooring design for the FOWT is governed by bending restrictions of the export electricity cable, the WT acceleration limits imposed by the vessel motions (pitch and roll) and the seabed conditions (Ma et al., 2019). Design codes for the mooring systems are

detailed in guidelines by American Bureau of Shipping ([FOWT Installations](#), updated 2018) DNV-GL ([DNVGL-ST-0119](#), 2018) and Bureau Veritas ([NI572 R02](#), 2019).

The TLP is not suitable for sites with high tide ranges since the legs need to be tensioned at all times. If this condition cannot be fulfilled, high snap loads will occur at times when the line re-tensions again. This will lead to instant or eventual failures (Handerson et al., 2016). The TLS has smaller a footprint on the seabed compared to the catenary mooring. Special anchors which can withstand vertical loading are needed for the TLS. This limit the suitable sites for TLPs depending on the seabed composition, the most used type is the suction anchor. On the other hand, in the case of the catenary mooring the forces on the anchors prevail in the horizontal directions. The most used anchor type for catenary lines is the drag anchor.

Table 6 - Characteristics of different mooring concepts (González & Diaz-Casas, 2016)

Type	Characteristics
Taut spread mooring	<ul style="list-style-type: none"> • Small footprint • Vertical loading at anchoring point • Large loads placed on the anchors—requires anchors which can withstand large vertical forces • Very limited horizontal movement • High tension limits floater motion (pitch/roll/heave) to maintain excellent stability • Challenging installation procedure • Minimal disruption to the seabed (small footprint)
Catenary mooring	<ul style="list-style-type: none"> • Large footprint • Horizontal loading at anchoring point • Long mooring lines, partly resting on the seabed, reduce loads on the anchors • Some degree of horizontal movement • Weight of mooring lines limits floater motion, but greater freedom of movement than taut-leg • Relatively simple installation procedure • Lower section of chain rests on the seabed, resulting in more disruption (large footprint)
Semi-taut mooring	<ul style="list-style-type: none"> • Medium footprint • Loading typically at $\sim 45^\circ$ to anchoring point • Medium loads on the anchors • Limited horizontal movement, but full structure can swivel around the turret connection • Single connection point makes the platform susceptible to wave induced motion • Relatively simple installation procedure • Low level of disruption (medium footprint)

2.4. Fatigue Analysis of the FOWT

For alternating loads, a sinusoidal representation may be considered as the simplest form of loading history for the purposes of FA. To describe the average stress over a period of loading a mean stress (σ_m) is introduced. Mean stress is defined as average of the stress minima (σ_{min}) and the stress maxima (σ_{max}) from the history (equation 4).

$$\sigma_m = \frac{\sigma_{max} + \sigma_{min}}{2} \quad (4)$$

Absolute difference between σ_{max} and σ_{min} is termed range. Amplitude of the stress history is defined as a half of the range of the recorded values as indicated in equation (5):

$$\sigma_a = \left| \frac{\sigma_{max} - \sigma_{min}}{2} \right| \quad (5)$$

(Sutherland, 1999).

Data determining the fatigue data are collected through specimen testing. A collection of data from a constant-amplitude fatigue tests is commonly called S-N data. These sets represent the number of cycles (N) at the stress/strain levels (S) to fail the sample. S-N curves are a representation of the information collected. S-N curves or so called Wöhler curves are commonly used in industries to determine the fatigue life of structures (Sutherland, 1999). Researchers agree that this kind of technique does not provide the desired precision of fatigue estimations and various improvements to the method were introduced (Susmel & Lazzarin, 2002).

A rainflow counting method is now established as a general and easy to apply practise for fatigue calculations across industries. The wind energy sector is not any different in this aspect. The rainflow counting analysis combined with Miner's rule is widely applied. The rainflow analysis was developed by Endo and Matsushi in 1968. The method has its name due to the similarities between rain flowing down the pagoda roof and the method of loading cycle counting. In the original method the recorded stress-time history plot is rotated 90°clockwise and the cycle counting is performed as defined in Lee et al. (2011) in Chapter 3:

- After the plot rotation, imagine a flow of water starting at each successive extremum.
- Let the water drip down the roof to establish half-cycles until:
 - *It falls opposite a larger maximum (or smaller minimum) point;*
 - *It meets previous flow falling from above;*
 - *It falls below the "roof".*
- Hysteresis loop is identified by pairing up the same counted reversals.

(Lee et al., 2011, page 91-92).

Various improvements were made to the original technique and several extensions of the original method exist. Figure 15 depicts the method on a random loading sample with the creation of the hysteresis diagram.

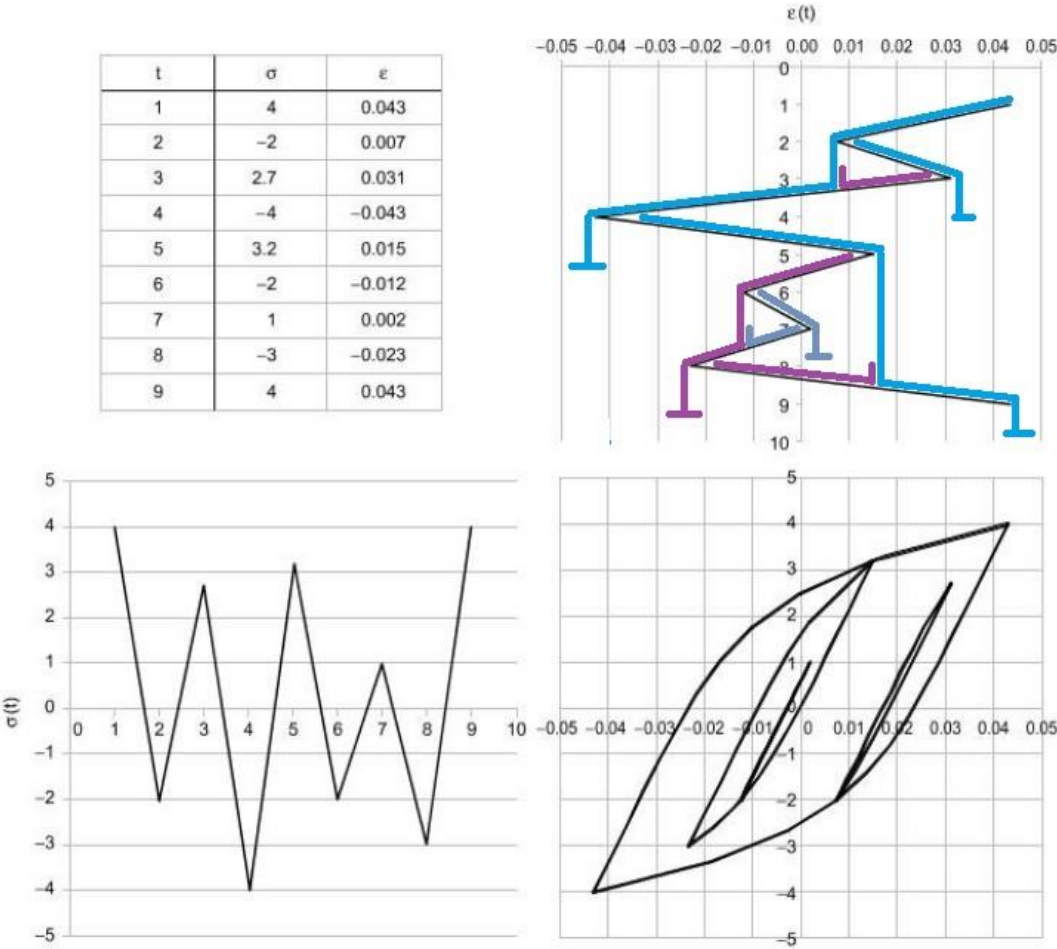


Figure 15 – Rainflow method performed (top right); hysteresis loop of data (bottom right) (Lee et al., 2012)

The international standard IEC 61400, 2019 edition is not strict about which technique should be used for fatigue calculations. The Miner’s rule is mentioned in the general part 1 of the edition. This law states that the final damage sustained (D) is a sum of the number of stress cycles sustained by the structure (n_i) over the number of the same stress cycles leading to failure of the structure (N_i) and can be written as:

$$\sum_i^M \frac{n_i}{N_i} = \frac{n_1}{N_1} + \frac{n_2}{N_2} + \frac{n_3}{N_3} + \dots + \frac{n_M}{N_M} = D \tag{6}$$

A foundation report “On the Fatigue Analysis of Wind Turbines” by Sutherland (1999) a very important point is highlighted: “...differences of a factor of 2 between damage predictions and measured lifetimes are not only common in wind turbine applications, they should be

expected.”(p. 5). This is due to the uncertainties of variations in loading on the wind turbine and the variations of the material properties. The accuracy of the FA is highly dependent on the technique and distribution representation of the load selected. More on this will be discussed in [2.5](#). It should be noted that the distribution representation can have important high stress events in the tail and some distributions are unable to represent this accurately/omit these events.

The more recent work focused mostly on the fatigue analysis of the HAWT applications in FOWT include extensive studies on the global structural fatigue taking into account coupled wave-wind dynamics. It was proven by several studies (Jonkman, 2007; Chen, 2017) that decoupled modelling of the two leads to the underestimation of the loads. The blade fatigue analysis was of a great interest to the industry since the early developments of onshore wind and the studies have proven useful in offshore applications. Chen & Basu (2018) focused the research work on fatigue effects of coupled wave-current dynamics on a SPAR supported HAWT. It was proven, that non-consideration of the current forces leads to miscalculation of fatigue life of the mooring cables and that wave-current interaction has some but limited influence on the fatigue life of the structure. Li et al. (2018) in their fatigue analysis of the bottom of the tower of the WT used the rainflow counting method.

2.5. Modelling Approaches

Modelling codes for the FOWT applications are extremely complex. The physics of the problem include aerodynamics, hydrodynamics, structural dynamics and mooring dynamics. The basic two approaches are numerical and experimental. In the validation stage of the numerical methods both approaches go hand in hand. Each of the dynamics problems has various methods for solving. There are simple linear models, which can be applied only to restricted simplified methods and are usually used as the first estimation. These methods are easy to solve for and do not require much of computational power. For more accurate modelling computational fluid dynamics (CFD) methods using non-linear equations are available. The detailed modelling options for each of the dynamics problems are described with detail in Matha et. al. (2016).

It was proven by Matha et al. (2009) that time-domain modelling approach is more suitable for study of the behaviour of the FOWT due to the complicated couplings of the system and its effect on the natural frequency estimations of the system. The frequency domain analysis widely used in the offshore oil and gas industry can offer accurate estimations of the supporting structure hydrodynamic responses; however, it is not as accurate for modelling of

the coupled dynamics of the complex system such as FOWT for reasons outlined above (Matha et al., 2016). It was also proven that the hydrodynamic loading and aerodynamic loading should be considered together, as a superposition of the terms underestimates the final loading greatly.

This led to development of several different software packages which can handle such complicated tasks. The available software which can solve coupled tasks comes from different companies and institutions. Most of the codes have been specially developed for the calculations of responses of WT. The most popular within the R&D in the wind energy industry is the FAST (Fatigue, Aerodynamics, Structures, and Turbulence) tool developed by NREL (Jonkman et al., 2005). This code is an open source package now also offered as OpenFAST version, claiming to be more user-friendly. This code is based on multibody dynamics in combination with modal methods. The modal methods use reduced number of degrees of freedom (DoF) when compared to the finite element methods. Non-linear loading can be applied through the code; however, the modal methods do not allow for material non-linear behaviour and geometrical stiffening to be considered. This code is popular due to its computational efficiency. The disadvantage of the modal methods in general is the requirement of very accurate pre-processing. (Matha et al., 2016).

SIMPACK developed for general mechanical engineering purposes for multibody system calculations and is widely used by the range of industries from automotive to robotics. This code is capable of doing all the calculations required for floating HAWT design and evaluation.

DNV-GL developed a code for land based WT – Bladed, which was then extended to be able to evaluate the FOWT, lately DNV-GL also supply the MARINTEK SIMA software using the combination of SIMO and RIFLEX codes. SIMA will be further described in section [3.1](#).

Reliable VAWT models in industry are lacking and models are usually created with in-house codes. Marintek SIMA provides a basic model of Darrieus rotor. A code for analysis of VAWTs is being developed at the University of Cranfield, UK. This code is specially designed for the VAWT concept; the lead researcher is Dr. Borg. As a summary a table of codes available and the methods of calculations these use are below in [Table 7](#). The table also contains codes which are not mentioned in the above paragraphs and the reader is referred to Cordle & Jonkman (2011) and Robertson et al. (2014).

Table 7 - Numerical codes summary table (Robertson et al., 2014)

Code	Developer	Structural dynamics	Aerodynamics	Hydrodynamics	Mooring model
FAST v8	NREL	T: Mod/MB P: Rigid	(BEM or GDW) + DS	PF + ME	QS
SIMPACK + HydroDyn	SIMPACK	T: Mod/MB P: Rigid	BEM or GDW	PF + QD	QS
Bladed (Advanced Hydro Beta)	DNV GL	T: Mod/MB P: Rigid	(BEM or GDW) + DS	PF + ME + (IWL)	QS
Simo, Reflex + AeroDyn	MARINTEK, NREL	T: FE P: FE	(BEM or GDW) + DS	PF + ME	FE/Dyn
HAWC2	DTU Wind	T: MB/FE P: MB/FE	(BEM or GDW) + DS	ME	FE/Dyn

The nomenclature for the [Table 7](#) above is as follows: T – turbine, P – platform. Mod – modal, MB – multibody, FE – finite element, BEM – blade element/momentum, GDW – generalised dynamic wake, DS – dynamic stall, PF – potential flow, ME – Morison’s equation, QD – quadratic drag, IWL – instantaneous water level, QS – quasi-static, Dyn – dynamic.

3. Model Description

This chapter gives details on the software, techniques and model used.

3.1. Software used

As it was mentioned in [2.5](#), there are various codes available for modelling of the FOWT. Initially the NREL's code OpenFAST was intended to be used. This software is based on its previous version FAST and is widely applied by the wind energy industry. The code is open-source and suitable for modelling of onshore based as well as offshore based HAWTs. One major shortcoming of using this code for this work is its inability to model VAWTs. It was decided to use the MARINTEK's SIMA software instead. This commercial software was designed to handle modelling of marine operations and floating systems. The package relies on non-linear FE for modelling of the multibody systems in time domain. This code offers handling of offshore floating HAWTs as well as VAWTs through the SIMO & RIFLEX coupled tasks.

To obtain hydrostatic data for the floating support of the VAWT concept, the spar was first modelled in SESAM GeniE and then analysed using the SESAM HydroD module. GeniE is a DNV-GL modelling tool using FEM and it is further enabled to analyse fixed offshore structures. It can be used to model bodies which can be like in this case exported to other parts of the package for further analysis. The file mesh was exported to the HydroD software where a hydrodynamic analysis was conducted with model based on the potential flow theory.

3.2. The Model

A model of 5MW HAWT on a spar buoy was established as the baseline scenario. A VAWT buoy was studied to compare the fatigue at the bottom of the tower. Both scenarios were studied under the same environmental loading. This section describes the models studied during this work.

3.2.1. Environment

Environmental conditions for all the models are the same. For the base line scenario, it was decided to consider wave and wind loading on the structure. To model the phenomenon spectral representation of the wave and wind was used. A JONSWAP 3-parameter spectrum was used to model waves and a Devonport spectrum to model wind. Three different sea state conditions were used – sea state condition 1 with significant wave height $H_s=6$ m and peak period $T_p=10$ s and probability of occurrence $p=0.2$; sea state condition 2 with $H_s=9$ m, $T_p=13.2$ s and $p=0.6$; sea state condition 3 with $H_s=12$ m, $T_p=14.5$ s and $p=0.2$. Compared to

the WMO sea state description, all three conditions are from the upper sea state range – indicating stormy sea conditions.

The Devonport spectrum for the wind representation was selected with the mean wind speed $v_{\text{meanwind}}=15$ m/s. The wind characteristics for the three sea states were assumed to be the same. The author is aware that this does not fully represent the reality; however, due to the time limit this simplification was adapted. In the second scenario a current in the same direction as wind was added. The IEC 61400-3-2:2019 urges to count the current loading during fatigue calculations. Not doing so can, as explained in Chen & Basu (2018), lead to serious misestimating of fatigue life. The defined current had speed varying between 4 and 5 m/s in the 10 to 15 m below the still water line (SWL) coming from 0° and 180° direction respectively for second and third sets of scenarios. The conditions are summarized in the Table 8 and the defined current profile and wave and wind spectral representations are in Appendix 1.

Table 8 - Environmental Conditions Summary

Wave conditions	Spectrum	Significant Wave Height (H_s)	Peak Period (T_p)	Probability (p)	Direction
Sea State cond.1	JONSWAP 3	6 m	10 s	0.2	0°
Sea State cond.2	JONSWAP 3	9 m	13.2 s	0.6	0°
Sea State cond.3	JONSWAP 3	12 m	14.5 s	0.2	0°
Wind conditions	Spectrum	Mean Wind Speed (v_{meanwind})	-	-	Direction
Wind cond. 1	Devonport	15 m/s	-	-	0°
Current conditions	Depth 1	Velocity 1	Depth 2	Velocity 2	Direction
Current 1	10 m	4 m/s	15 m	5 m/s	0°
Current 2	10 m	4 m/s	15 m	5 m/s	180°

3.2.2. Basic Model

It was decided to use the IEA Annex XXIII Offshore Code Comparison Collaboration (OC3) Phase IV spar buoy as the support for the HAWT. This floater was developed based on the Hywind project and the support's model is freely available with hydrostatics and hydrodynamic responses calculated. Jonkman (2010) reports detailed properties and results of the calculations carried out for the floater. The buoy was designed to carry a 5-MW Reference Wind Turbine for Offshore System Development proposed by the NREL and commonly known as "NREL 5MW". This turbine is mounted on the top of the OC3 Phase IV spar. The hub is mounted on the 87.6 m high tower. It is an upwind WT with three blades. The swept area after the correction for the effect of blade precone is $A_s=12\ 445.3\ \text{m}^2$. The correction is calculated as:

$$A_s = D^2 * \cos(\alpha) * \frac{\pi}{4} \quad (6)$$

Where D is the turbine diameter and α is the angle of blade precone, the precone for this WT is $\alpha=2.5^\circ$. The regime of the wind turbine was specified as follows: cut in speed $s_{\text{cut-in}1}=3\ \text{m/s}$; rated speed $s_{\text{rated}1}= 11.4\ \text{m/s}$ and cut-out speed $s_{\text{cut-out}1}=25\ \text{m/s}$. The hub mass is defined as $M_{\text{hub}}=56780\ \text{kg}$ with mass moment of inertia calculated to be $I_{xx_hub}=115926\ \text{kg/m}^3$ (hub being simplified as a spherical shell $r=1.75\ \text{m}$), from:

$$I_{xx_hub} = \frac{2}{3} M_{hub} r^2 \quad (7)$$

The spar has following dimensions: depth 120 m with the centre of gravity 30.08 m above the baseline. The floater has three different sections – the bottom cylindrical part has depth $h_{b1}=108\ \text{m}$, radius $r_{b1}= 4.75\ \text{m}$; the top cylindrical part has depth $h_{t1}= 4\ \text{m}$, radius $r_{t1}= 3.25\ \text{m}$; the taper part connecting the bottom and top cylinders has depth $h_{c1}=8\ \text{m}$. The thickness of the walls of the cylinder is not given in the report.

The all dimensions and other specifications are listed in the Table 9.

Table 9 - Base line WT specifications

Centre of gravity	30.08 m (above keel)	Centre of buoyancy	
Spar	Depth	Radius	Thickness
Bottom cylinder	108 m	4.75 m	unknown
Taper	8 m	4.75 - 3.25 m	unknown
Top cylinder	4 m	3.25 m	0.027 m

Table 9 continued - Base line WT specifications

-	Height	Radius	Thickness
Tower	87.6 m	3.25 – 1.935 m	0.027 – 0.019 m
-	Mass	Moment of inertia	Radius
Hub	56780 kg	115926 kg/m ³	1.75 m
-	Swept Area	Rated Power	Blade length
Turbine	12 445.3 m ²	5 MW	61.5 m
-	Cut-in	Rated	Cut-out
Operation Speed	3 m/s	11.4 m/s	25 m/s

3.2.3. Two blade HAWT model

The two bladed horizontal wind turbine was defined based on average data of two bladed wind turbines compared to three bladed wind turbines as data for a two blade WT of 5MW were not available to the author. Major inspiration was the 4MW Hamilton Standard WTS-4 wind turbine. This turbine cut-in wind speed $s_{cut-in2}=6.9$ m/s; the WT performance was rated at $s_{rated2}=15.1$ m/s and operational limit speed $s_{cut-out2}=27$ m/s (Bussolari, not dated). The turbine has free yaw to align with the wind direction. Height and swept area is based on the 4MW Hamilton WT, height of the tower is 77.6 m and the swept area $A_{swept2}=5026$ m². As the swept area is smaller a more potent generator needs to be placed to maintain the same power extracted. The hub mass and mass moment were adjusted to the fact that the rotor has only two shorter blades but contains bigger generator as $M_{hub2}=53000$ kg and $I_{xx_hub2}=108210$ kg/m³. The properties are summarized in the Table 10 below.

Table 10 - Properties of the two blade HAWT model

Centre of gravity	30.08 m (above keel)	Centre of buoyancy	
Spar	Depth	Radius	Thickness
Bottom cylinder	108 m	4.75 m	unknown
Taper	8 m	4.75 - 3.25 m	unknown
Top cylinder	4 m	3.25 m	0.027 m
-	Height	Radius	Thickness
Tower	77.6 m	3.25 – 1.935 m	0.027 – 0.019 m
-	Mass	Moment of inertia	Radius
Hub	53000 kg	108210 kg/m ³	1.75 m

Table 10 continued - Properties of the two blade HAWT model

-	Swept Area	Rated Power	Blade length
Turbine	5026 m ²	5 MW	38.2 m
-	Cut-in	Rated	Cut-out
Operation Speed	6.9 m/s	15.1 m/s	27 m/s

3.2.4. VAWT model

The initial intended turbine for this thesis was a H-rotor based on the research work of Hand & Cashman (2017). However, due to the limited time available a 5MW Daerrius rotor developed for the DeepWind project, based on the work of Vita (2011) was chosen for the purpose of this work.

The draught of the floater is 108 m with the centre of gravity 27.84 m above the baseline. The floater has three different sections – the bottom cylindrical part has depth $h_{b2}= 93$ m, radius $r_{b2}= 4.15$ m and wall thickness $t_{b2}=0.05$ m; the top cylindrical part has depth $h_{t2}= 5$ m, radius $r_{t2}= 3.15$ m and wall thickness $t_{t2}=0.02$ m; the taper part connecting the bottom and top cylinders has depth $h_{c2}=10$ m and thickness $t_{c2}=0.05$ m. The rotor height is 129.56 m and its radius is 63.74 m, the swept area is $A_{swept3}=10743$ m². The 5MW generator is located at the bottom of the tower, at the WL. The dimensions are listed in the Table 11. Complete description of model used can be found in Vita (2011).

Table 11 - VAWT model specifications

Centre of gravity (CG)	27.84 m (above keel)	Centre of buoyancy	18.57 m (above CG)
Spar	Depth	Radius	Thickness
Bottom cylinder	93 m	4.15 m	0.05 m
Taper	10 m	4.15 - 3.15 m	0.05 m
Top cylinder	5 m	3.15 m	0.02 m
-	Height	Radius	Thickness
Tower	145 m	3.15 m	0.02 m
Rotor	129.56 m	63.56 m	-
-	Swept Area	Rated Power	Blade length
Rotor	10743 m ²	5 MW	188.68 m
-	Mass	Moment of inertia	Height
Total	5.64 10 ⁶ kg	1.87 10 ¹⁰ kg/m ³	108 m + 145 m
-	Cut-in	Rated	Cut-out
Operation Speed	5 m/s	14 m/s	25 m/s

4. Modelling

Creation of a reliable model based on the specifications is vital for every real-world simulation. Step description of the model development in the selected software is given in this chapter.

4.1. Structural and Hydrodynamic modelling

To obtain important input data for the spar buoy for the VAWT model additional simulations were required. The structural model was generated based on the data above in the SESAM GeniE. The mesh element length was set to 1 m, which given the geometry simplicity allows for rather accurate results. There are two different approaches to model a spar. A shell model was selected and created from three cylindrical sections and a shell plate at the bottom with the dimensions described in [3.2.4](#). The second possible model would feature beam elements with a pipe-like cross-section to account for the wall thickness. The mesh was saved as a .FEM file and exported to the SESAM HydroD. A panel model for Wadam Wizard run was created to obtain hydrodynamic data. For the hydrodynamic calculations set of direction from which the waves are incoming is needed to be created. For a cylindrical symmetric structure one direction of incoming waves is enough. A set of wave frequencies is next to be established. The structure has a characteristic dimension (diameter $D=6.3$ m), which means the reasonable wave frequency set is between 0.01 and 8 rad/s (Yuan, 2018). This is the range of frequencies to cover all the important frequency responses of the structure. Considering the diameter of the structure it is known from literature this range is enough for convergence. The mesh generated in SESAM GeniE and the SESAM HydroD hydrostatic model is documented in the Figure 16 - GeniE generated mesh and HydroD model.

The panel model was used due to the writer's preference; however, a Morrison model would be also suitable for this structure. The panel method is a boundary element method based on potential flow theory, which solves partial differential equations which can be expressed as integral equations. Different types of panel methods exist and are closely reviewed in Hess (1990) and Cruz (2009). The downside of the theory is its restrictions on the fluid and flow properties and the inability to calculate drag of the body (d'Alembert's paradox) (Batchelor, 2000).

GeniE Mesh



HydroD model

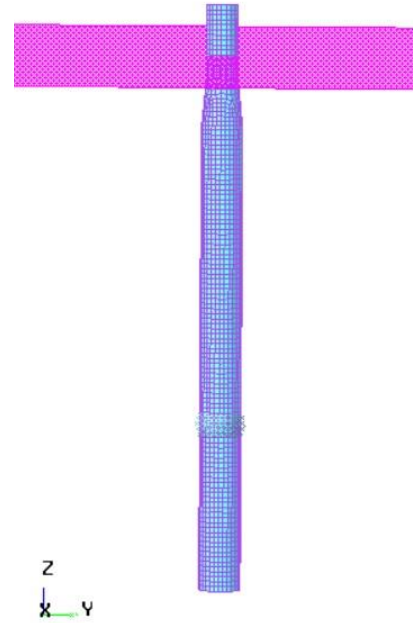


Figure 16 - GeniE generated mesh and HydroD model

On the other hand, the Morison model is suitable only for slender structures, which diameter is less than 0.2 of the wave length (λ). The Morison model is mainly governed by inertia forces (F_I) and drag forces (F_D) and the diffraction caused by the body presence in the fluid is omitted. It can be expressed by the following equation (“Morison Equation”):

$$F = F_I + F_D = \rho C_m V \dot{u} + \frac{1}{2} \rho C_d A u |u| \quad (8)$$

Where C_m is the inertia coefficient obtained from equation (9); V is the volume of the submerged body; ρ is the density of the liquid – e.g. water; C_d is the drag coefficient; A is the reference area of the body perpendicular to the flow direction and u is the flow velocity.

$$C_m = 1 + C_a \quad (9)$$

C_a is the added mass coefficient and together with C_d is obtained from experimental measurements.

Both of the approaches are valid according to the DNV-GL Environmental conditions and Environmental loads (2017) as the D/λ is lower than 0.2.

As the last step in WADAM run, additional calculation requirements can be specified. The wave drift forces need to be calculated in addition to the basic set calculations.

The hydrostatic properties were obtained from the POSTRESP data postprocessor and entered to the SIMA software with the geometry file of the spar. In the stiffness matrix and the damping matrix only the terms on the main diagonal were entered. This simplification was possible to make due to the large ($\geq E+5$) difference to the rest of the values. The original matrices can be found in the [Appendix 2](#).

4.2. Coupled Hydro- and Aero-dynamic modelling

Once all the necessary for modelling values were obtained from previous step. New workspace was created in SIMA. The workspace included three coupled RIFLEX tasks to allow for coupled modelling. The first task was imported from the examples available – “ExampleFloatingWindTurbine”; which features a predefined model of the NREL 5MW HAWT mounted on the OC3 Hywind spar. The environmental conditions were specified as in defined in 3.2.1. This task was used as an introduction the SIMA software and to gain proper insight on the procedures.

In the body properties a definition of the “HUBMASS” was adjusted to match the details given in the model description. The 3D representation of this model can be seen in [Figure 17\(a\)](#). A simulation of three different sea states with corresponding winds were run and post processed. To explore further the points made by Chen & Basu (2018) second and third scenarios with currents were created. The results were compared and are presented all together in the following chapter.

A two blade downwind WT was created as specified in the model description. The first step was to select airfoils used to represent the blades. The following set of airfoils was selected: *S809*, *cyl1*, *cyl2*, *du40*, *du35*, *du30*, *du25*, *du21* and *naca64*. Each type of airfoil has different cross-section and different aerodynamic properties. Cross-sections have to be defined as one of the properties needed for the 3D model creation. The cross-sections were established for the tower sections, the blades, the shaft and the above water line level of the buoy. Detailed cross-section properties are attached in the [Appendix 3](#) together with other defining parameters for the downwind HAWT model.

To create lines representing the structure, supernodes defining the lines boundaries were required; the supernodes and its coordinates are in [Appendix 3](#). Line types were selected to finally create the lines themselves. In the line type creation dialog window the line type was matched with its cross-section and its length. The blades and tower had various segments with different cross-section defined and the shaft describing line type had a special mechanical joint assigned to represent the torque transfer in the gearbox. Having these properties defined,

lines could be now created. In the line definition dialogue ten lines were created. Table 12 below gives the list of the lines with descriptive parameters such as line type, end supernodes assigned and the resulting length of the line. It should be noted that the tower height stated in the specifications and in the table is not matching; this is due to the ten meters of spar body which is going above the WL characterized by the line *sparart*. A wind turbine had to be created in the slender body system. The specified two blade downwind HAWT and information about its controls were added. A special local element axis needed to be specified for the blades and tower; this required to specify the reference vectors given in the global coordinate system.

Table 12 - Lines specifications for two blade HAWT model

Name	Line Type	End1	End2	Length	Distance	Disabled
shaft	shaft_lt	sh_sn1	sh_sn2	1.0	0.99998	<input type="checkbox"/>
bl1ecc	bl_ecc	sh_sn1	bl1e_sn2	1.5002	1.5	<input type="checkbox"/>
bl2ecc	bl_ecc	sh_sn1	bl2e_sn2	1.5002	1.5	<input type="checkbox"/>
sparart	spardum	sparloc	towerlow	10.0	10.0	<input type="checkbox"/>
bl2foil	bl_foil	bl2f_sn1	bl2f_sn2	38.217	38.217	<input type="checkbox"/>
bl1foil	bl_foil	bl1f_sn1	bl1f_sn2	38.217	38.217	<input type="checkbox"/>
tower	tower_lt	towerlow	towerup	67.6	67.6	<input type="checkbox"/>
moor_1	m_line	tp_1	anchor_1	902.2	902.2	<input type="checkbox"/>
moor_2	m_line	tp_2	anchor_2	902.2	902.2	<input type="checkbox"/>
moor_3	m_line	tp_3	anchor_3	902.2	902.2	<input type="checkbox"/>

Two bodies had to be created to represent the body mass of the hub and the nacelle. The mass and the mass moment of inertia were entered through the “structural mass” dialogue window in the body section and drag coefficient. The quadratic wind coefficient was established zero as the wind shading was not included in the model. The bodies had to be connected with the rest of the system via slender body connection, specifying the connecting line and segment. This procedure was used to define the above the WL components of the structure.

To create the below the WL structure a .FEM model and the hydrostatic properties were imported. The same OC3 spar was used. It is important to point out that the spar should be modified for this wind turbine as it is lighter and the structure above the WL is generally not as high as the WT the support is intended to. This would likely require a shorter spar buoy, but this was not the scope of this work. The predefined model had to be rotated 90° as the model was created with a different coordinate system. The hydrostatic stiffness and damping are presented in the Appendix 2 and can be compared to the values obtained for the smaller spar. The stiffness in yaw is defined from the mooring line stiffness. Lines describing the spar sections have to be assigned. The final model created is depicted in the [Figure 17\(b\)](#).

A model of the Darrieus rotor is provided in the software. The Naca0018 airfoil is used to create the blades according to the specifications in [3.2.4](#). Supernodes for identification of end

of lines were added for the mooring lines, tower and shaft and cross-sections were created similarly to the two blade HAWT task. Six lines in total had to be created for this task; these are described in [Table 13](#). The local axis was created for the tower. The hub body was created on the waterline as a cylinder with the same diameter as the tower. Nacelle was created 75 m above the WL, which is in the middle of the tower height. This is due the mass representation of the rotor itself. Mass form the model description and zero quadratic wind coefficient were specified for the two bodies. The shaft containing the torque joint connects the two. The VAWT is connected to the nacelle body. Slender body connection must be made to the rest of the system.

Table 13 - Lines specifications for the VAWT model

Name	Line Type	End1	End2	Length	Distance	Disabled
shaft	shaft_lt	sh_sn1	sh_sn2	75.0	75.0	<input type="checkbox"/>
moor_1	m_line	tp_1	anchor_1	903.0	903.25	<input type="checkbox"/>
moor_2	m_line	tp_2	anchor_2	903.0	902.77	<input type="checkbox"/>
moor_3	m_line	tp_3	anchor_3	903.0	902.77	<input type="checkbox"/>
sparart	spardum	sparloc	towerlow	10.0	10.0	<input type="checkbox"/>
tower	tower_lt	towerlow	towerup	135.0	135.0	<input type="checkbox"/>

The spar model and its hydrodynamic specifications are imported from the .FEM file from the GeniE and results file from HydroD. Lines representing the spar sections are created within the body folder.

The final models are represented in the [Figure 17](#) – (a) three blade HAWT, (b) two blade HAWT and (c) VAWT.

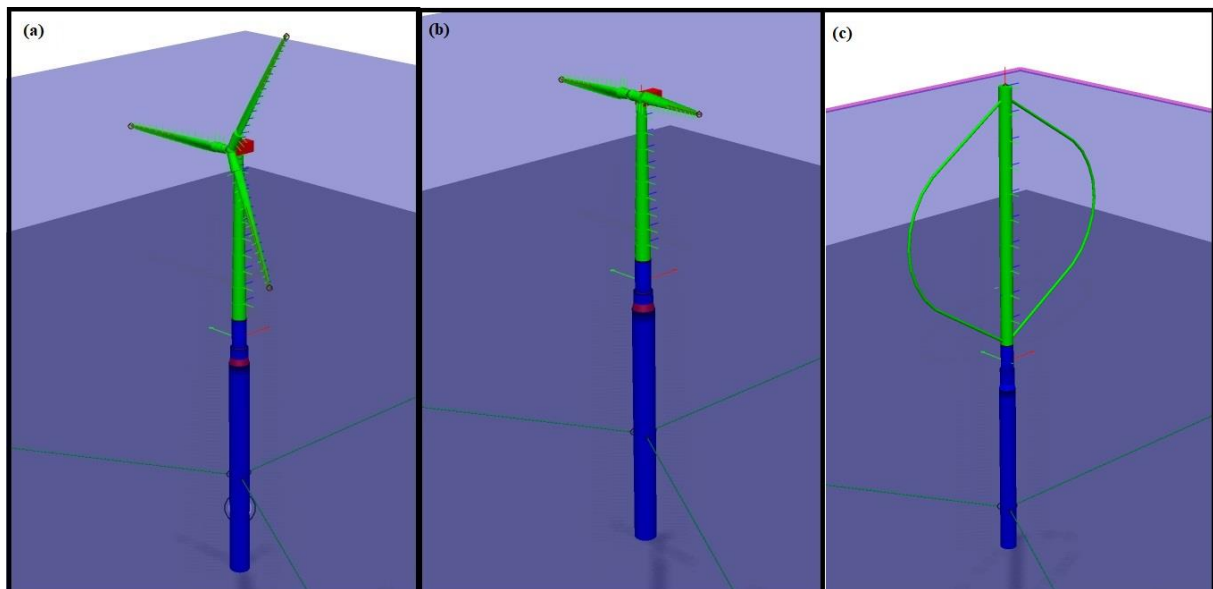


Figure 17 - The models of the turbines - (a) three blade HAWT; (b) two blade HAWT; (c) VAWT

The simulation was set to run for 250 s, 610 s and 1000 s with 0.05 time step. First 10 seconds of simulation were not counted into the results to avoid the start-up of the turbine. The

location for the two blade HAWT and VAWT had to be adjusted to accommodate the mooring lines. The new assigned water depth $D_{\text{water}}=320$ m. The environment for all the three models were specified as described in section [3.2.1](#).

4.3. Post-processing

To conduct fatigue analysis of the models a post-processing of the initial results must be done. The results obtained from the simulation before post-processing are of two natures – static results and dynamic results. Static results from the STAMOD module provide information on the displacement, force and moment data calculated from the static fixed parameter analysis. However, from the fatigue analysis (FA) point of view, the dynamic results from the DYNMOD module are more important. The DYNMOD calculated results for the given set of parameters in a time domain. These results contain important information for the FA, such as axial forces of the defined lines.

Creating the post-processing task in the SIMA will give access to further data analysis tools. The FA filters contain options such as axial stress estimation tools, pipe stress estimation tools and most importantly fatigue estimation tool. The fatigue filter will be used. This is a post-processing tool, which performs rainflow analysis as described by De Jonge (1970). The post-processed results then offer three outputs – damage, weighted damage and accumulated damage. Each of the outputs provides different information:

- *Damage* – gives damage for each component for each environmental condition
- *Weighted damage* – gives damage for each component for each environmental condition, weighted with the probability of occurrence
- *Accumulated damage* – sum of the weighted damage for each component.

(SIMA 64 V3.3-03 help tool)

Selected input to the post-processor will be the results calculated based on loading conditions for each scenario. Axial forces (F_A) at the bottom of the tower are selected as an input from the condition sets. The data will be then processed by an axial stress (σ_A) filter, where the axial forces will be transformed to axial stresses following:

$$\sigma_A = \frac{F_A}{A_F} \quad (10)$$

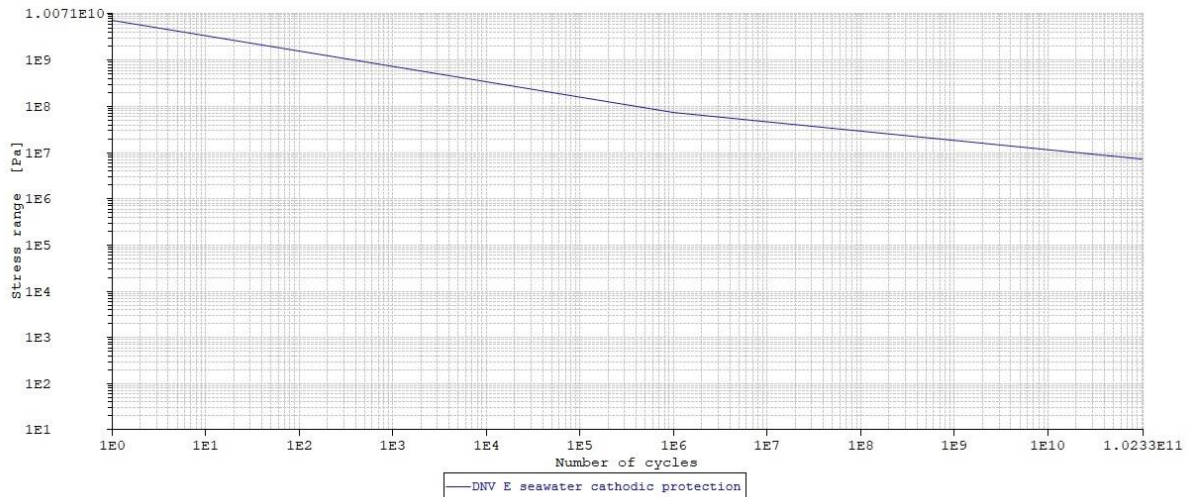


Figure 18 - S-N curve for DNV E grade steel with cathodic protection (DNV)

The area over which the forces act was estimated as $A_F = 0.549 \text{ m}^2$ for both HAWT scenarios, which is the area of the tower at its bottom with radius $r=3.25 \text{ m}$ and thickness $t=0.027 \text{ m}$ and $A_F=0.395 \text{ m}^2$ for the VAWT scenario, based on the tower radius $r=3.15 \text{ m}$ and thickness $t=0.02 \text{ m}$. An S-N curve (Figure 18) has to be specified. The material in question is DNV E grade steel with seawater cathodic protection. A fatigue filter will be then applied on the axial stresses calculated at the element 1 segment 1 of the tower. The result can then be plotted on screen or exported to a file. The layout of the post-processor is shown in the [Figure 19](#).

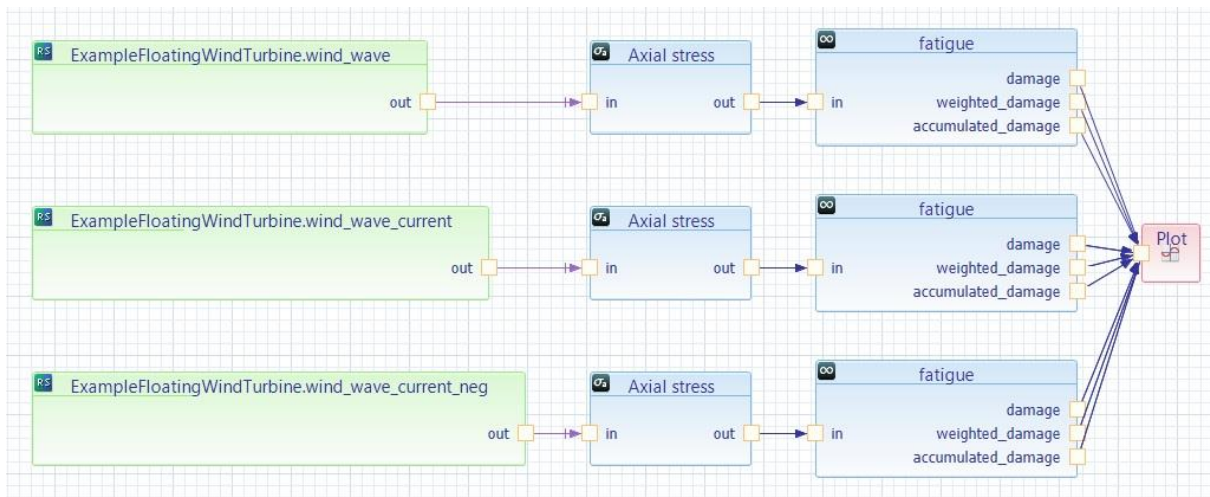


Figure 19 - Post-processor layout

5. Results

This chapter will present the results obtained through the modelling of the problem. The first section will provide results on all the scenarios with HAWT turbines, whereas the second part will concentrate on the results obtained based on the VAWT model. The results will be discussed in the next chapter.

Out of the three simulation lengths the results obtained through the 610 s long simulation will be presented and compared to the results of the 300 s simulation.

5.1. Three blade HAWT

The results of dynamic analysis for all the scenarios for the three bladed WT are presented below. First to show is the displacement variation between the three scenarios with the sea state condition 1. As it can be seen in the [Figure 20\(b\)](#), for the scenario with wind, wave and current coming from the same direction the displacement will be the greatest.

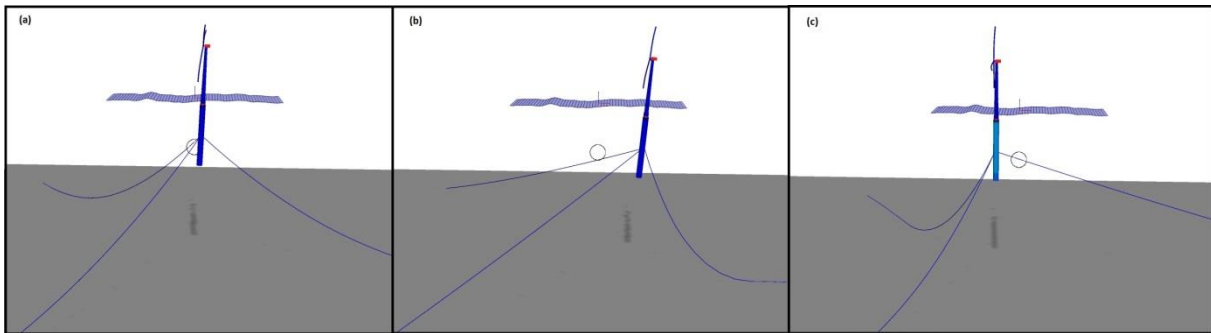
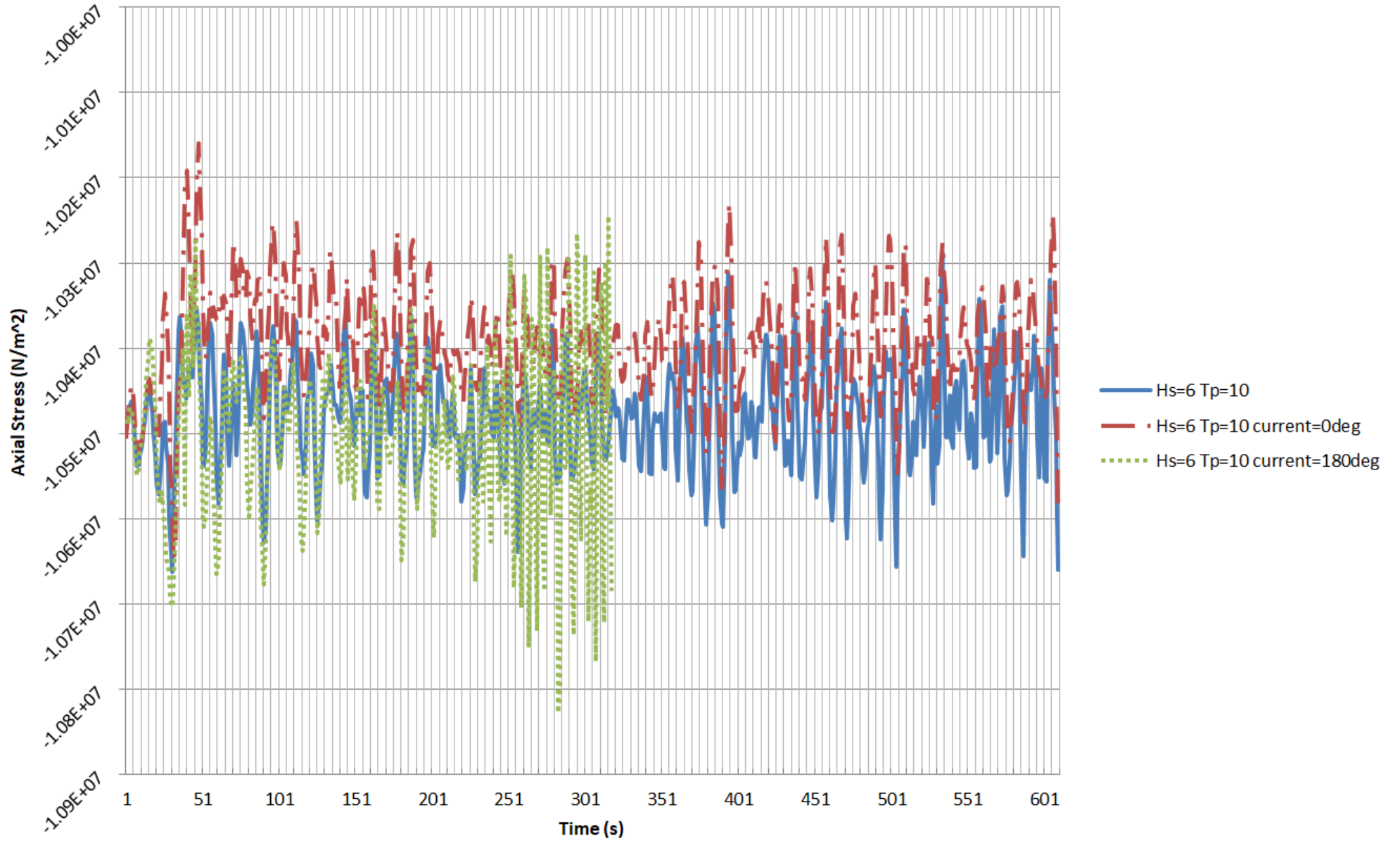


Figure 20 - Displacement of the FOWT depending on the scenario

The damage based on axial stresses and calculated on the tower will be presented by the matching basic environmental conditions e.g. wave height and peak period. Graphs for the damage occurred during the $H_s=6$ m and $T_p=10$ s. The results representation is in fatigue damage equivalent per event. The first 10 seconds of each simulation was cut off for the purposes of the FA as this data is corrupted by the start-up of the turbine.

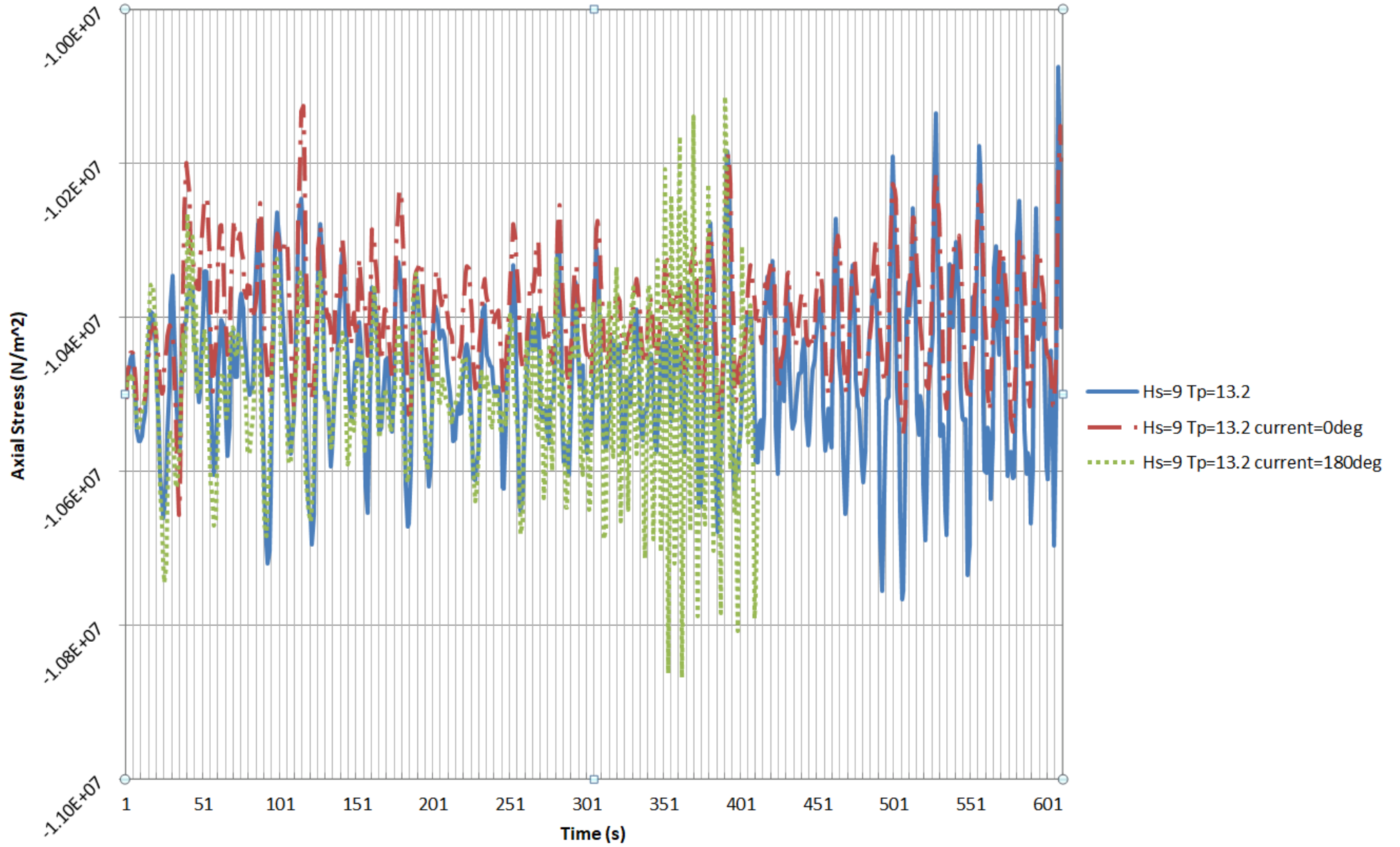
First, graphs of axial stress at the bottom of the tower for each scenario are presented (Graph 1, Graph 2 and Graph 3). Simulation of 610s was chosen as for the result representation. The fact the simulation for the most severe conditions with the opposing current was not completed will be discussed further in the next chapter.

Sea State Condition 1



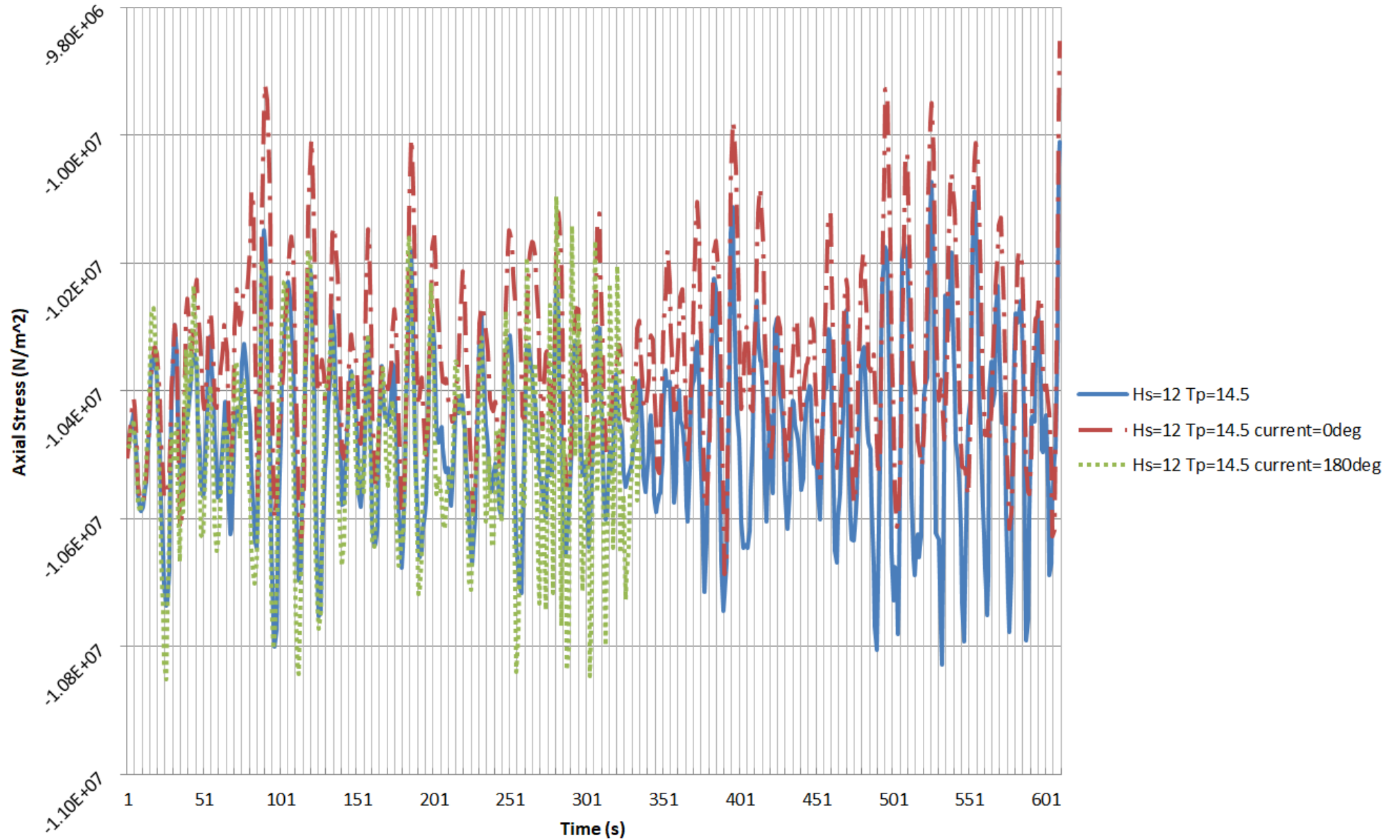
Graph 1 - Axial stress history for the Sea State Condition 1

Sea State Condition 2



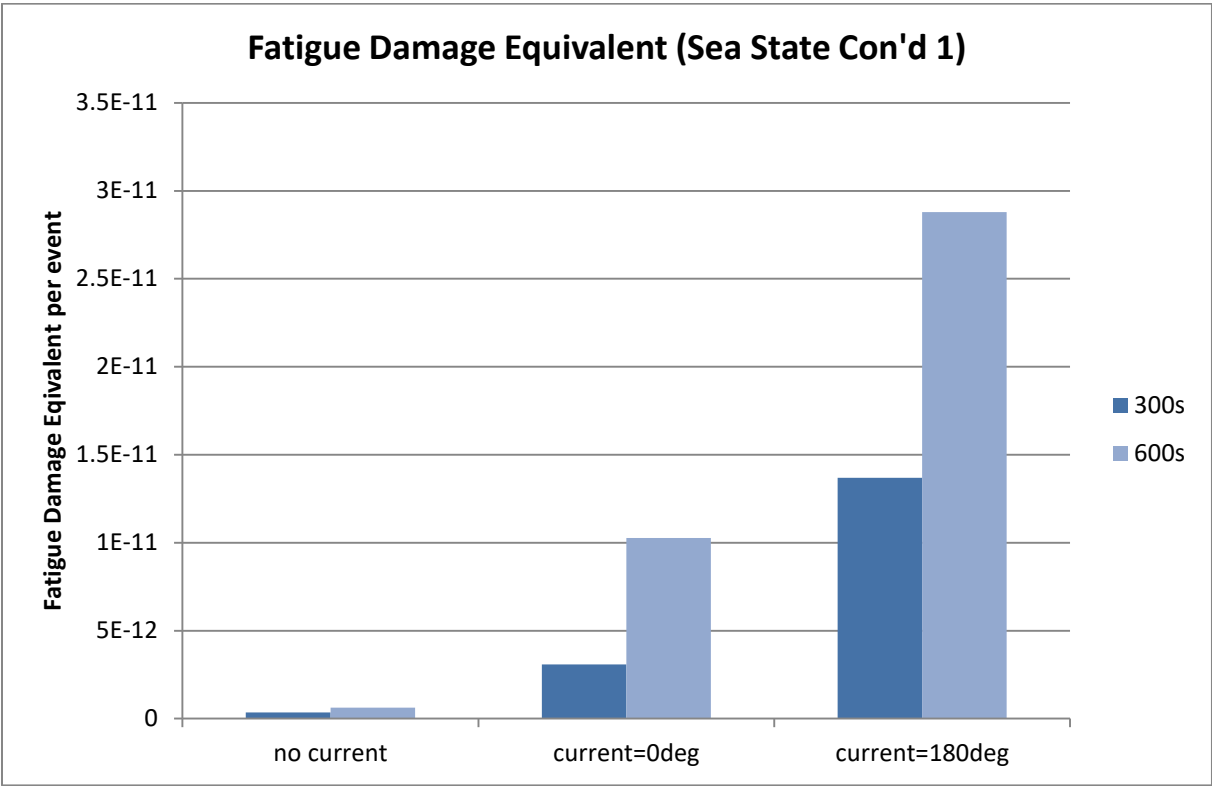
Graph 2 - Axial stress history for the Sea State Condition 2

Sea State Condition 3

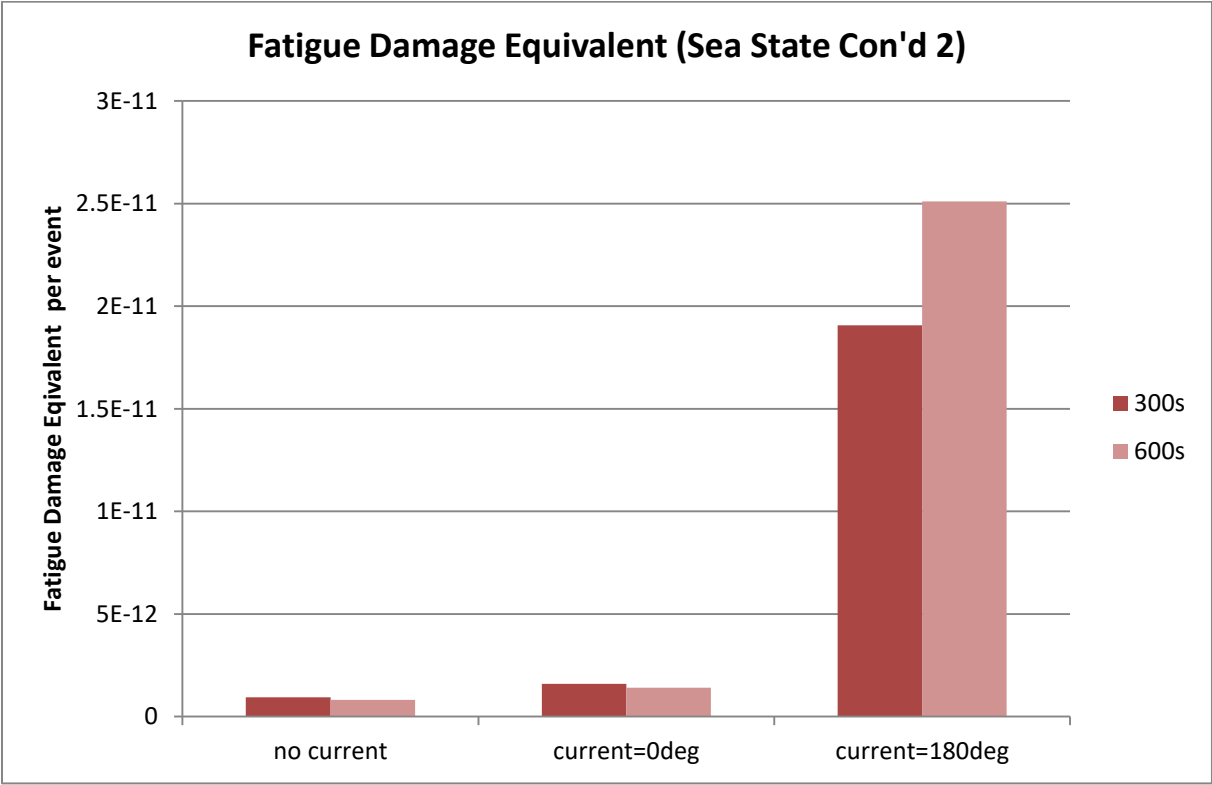


Graph 3 - Axial stress history for the Sea State Condition 3

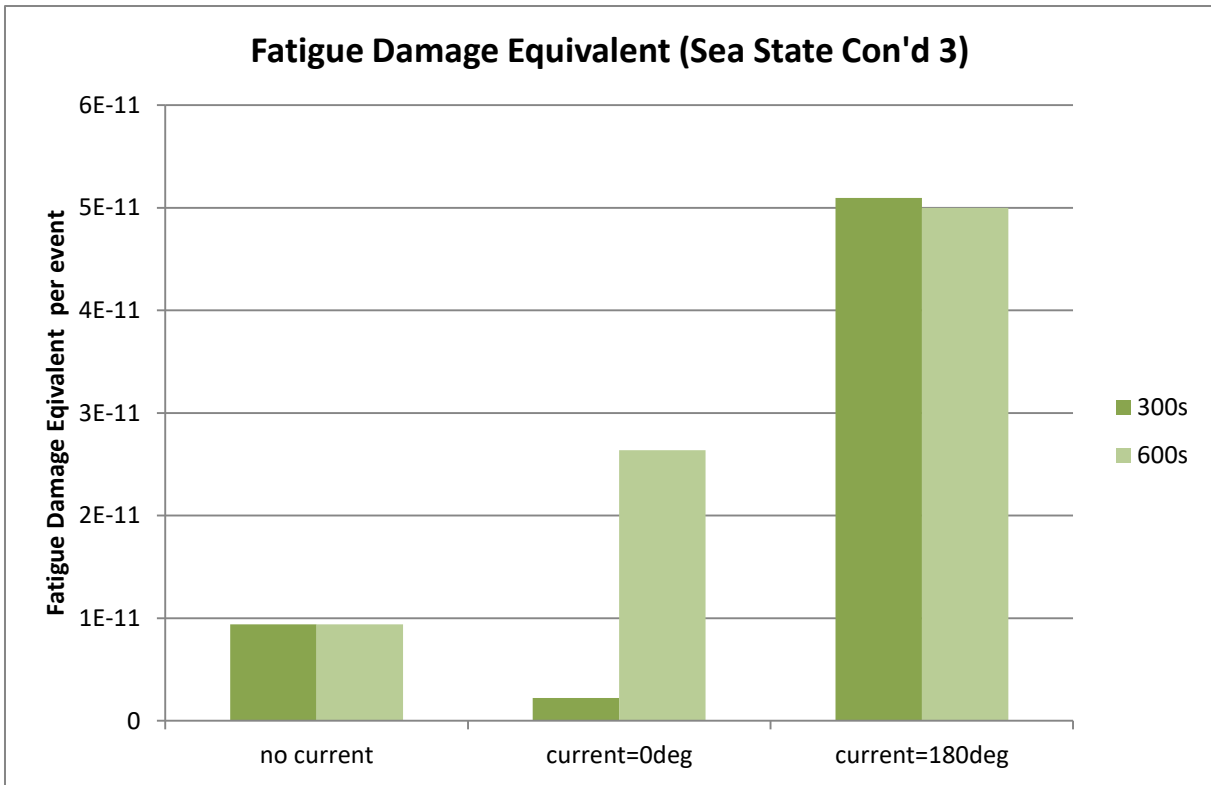
The damage equivalent results are presented in the Graph 4, [Graph 5](#) and Graph 6. Results for 300 s simulation and 600 s simulation are presented for comparison how a length of a simulation affects the difference in results obtained.



Graph 4 - Fatigue Damage Equivalent for Sea State Condition 1

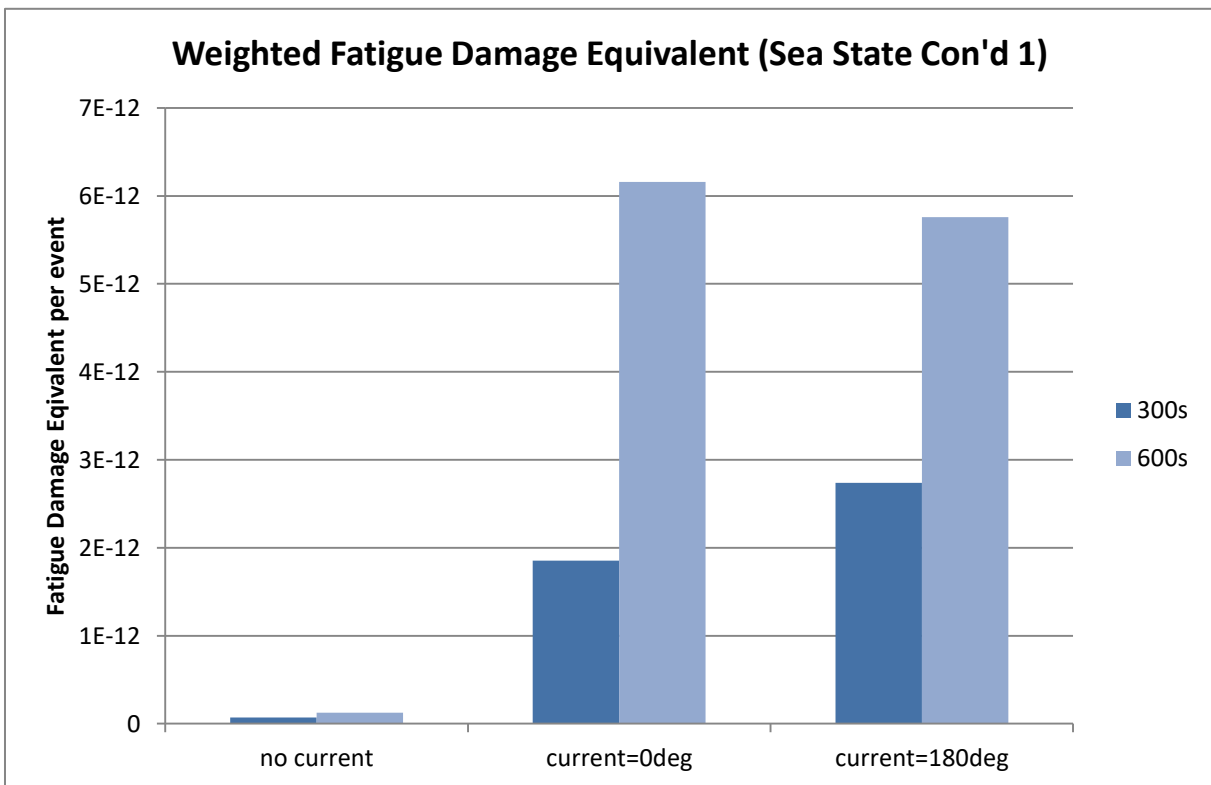


Graph 5 - Fatigue Damage Equivalent for Sea State Condition 2

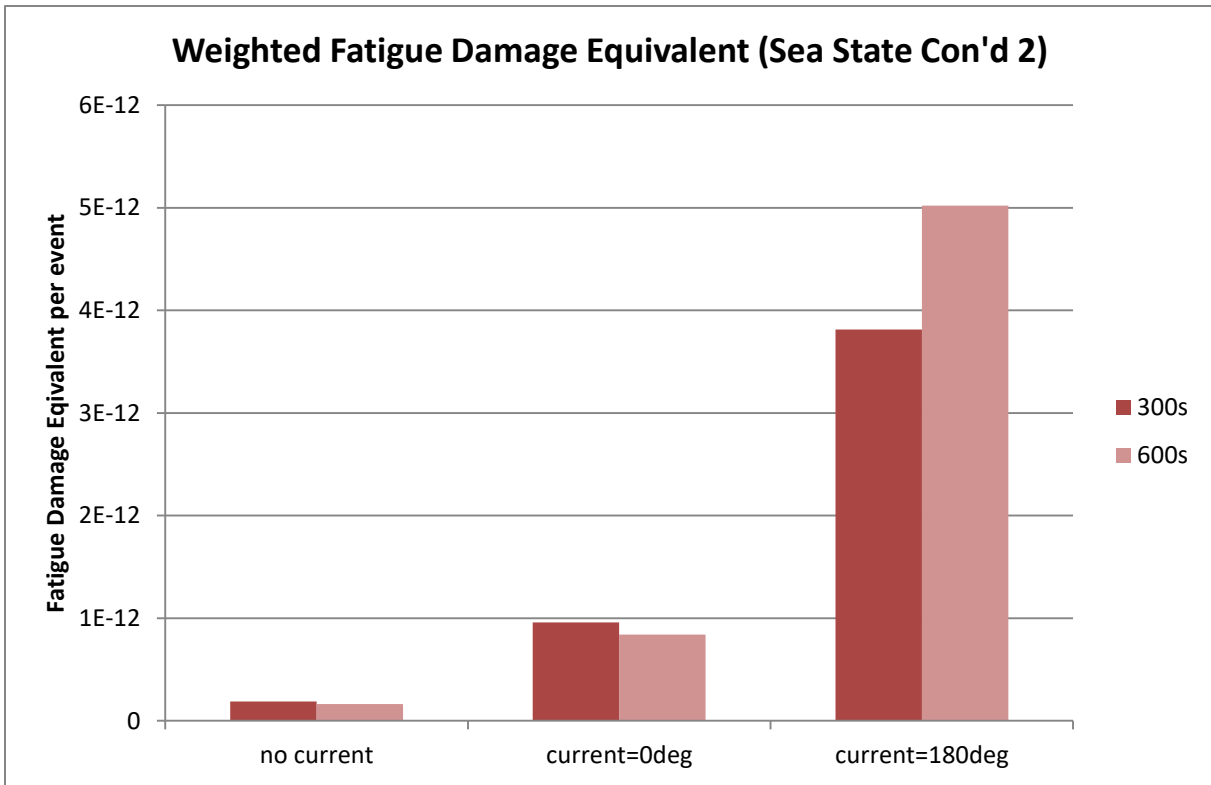


Graph 6 - Fatigue Damage Equivalent for Sea State Condition 3

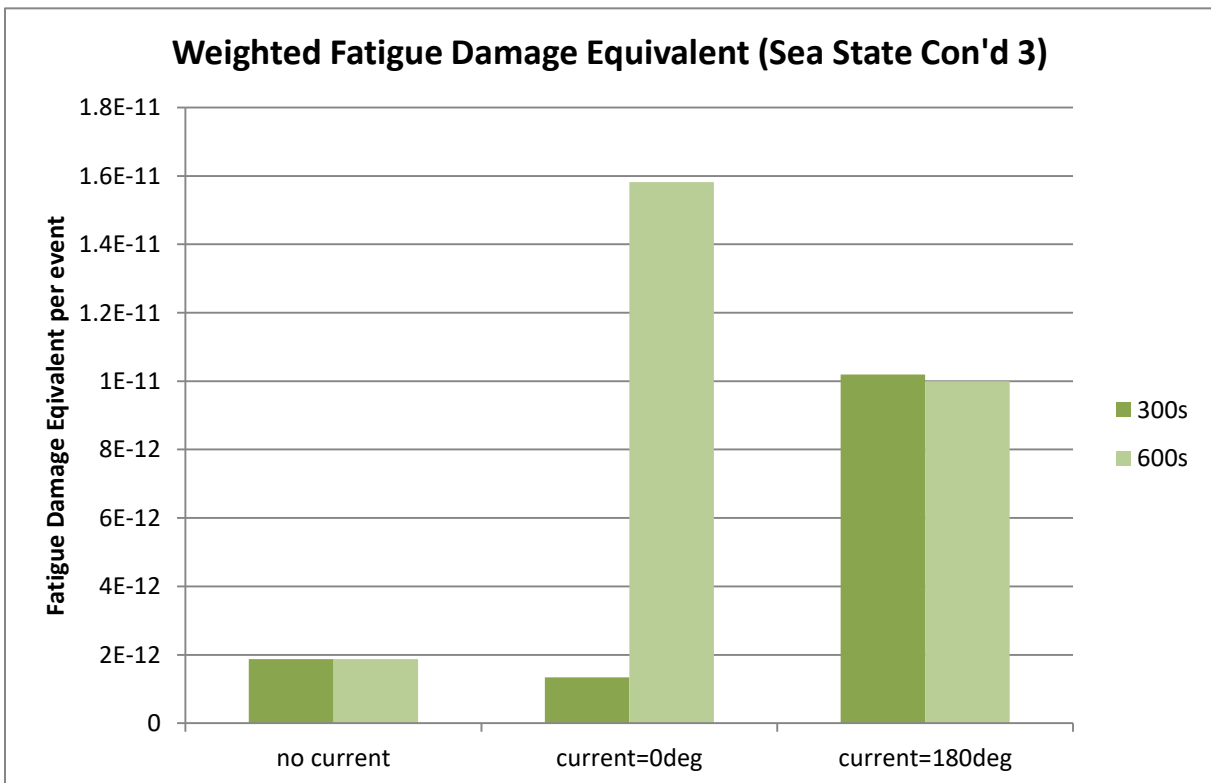
Weighted damage equivalent is presented in [Graph 7](#), [Graph 8](#) and [Graph 9](#) below. The probability of sea state conditions are as follows: $p_1=0.2$, $p_2=0.6$ and $p_3=0.2$.



Graph 7 - Weighted Fatigue Damage Equivalent for Sea State Condition 1



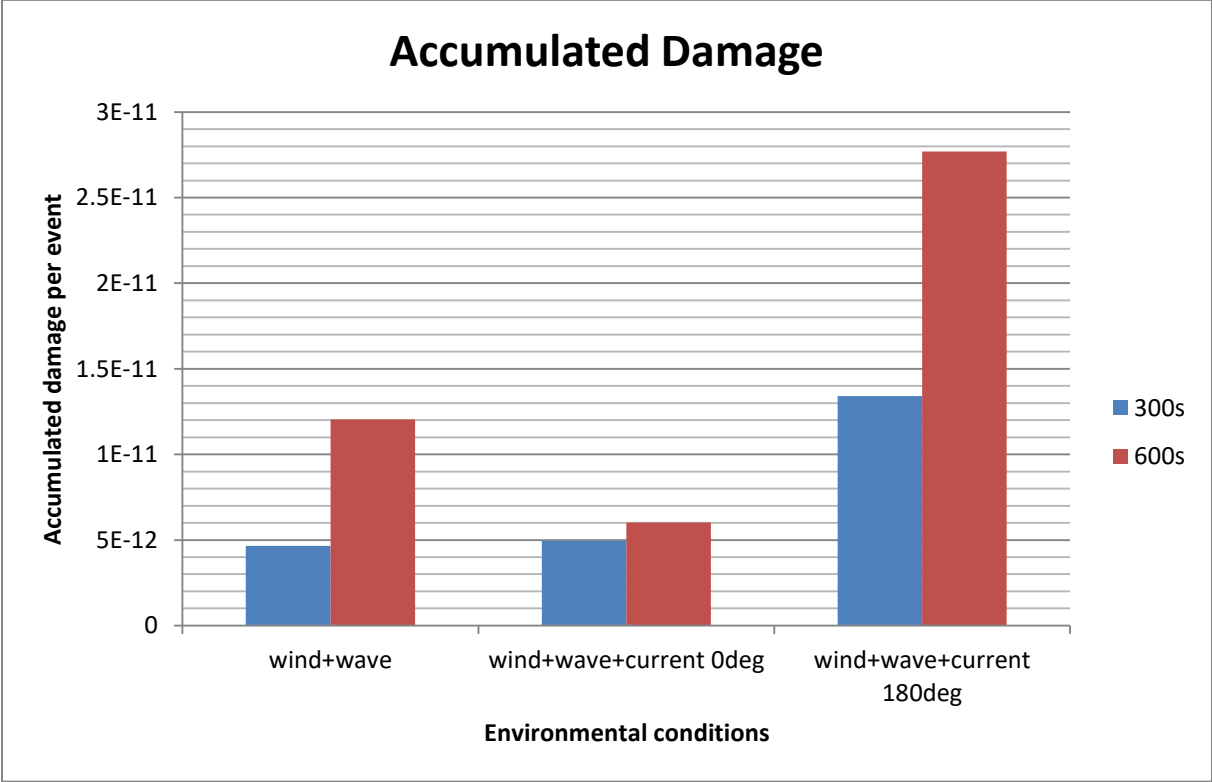
Graph 8 - Weighted Fatigue Damage Equivalent for Sea State Condition 2



Graph 9 - Weighted Fatigue Damage Equivalent for Sea State Condition 3

The Graph 10 shows the different fatigue damage sustained over the three different current scenarios – no current with probability $p=0.2$ of sea state condition 1 occurring, probability

$p_2=0.8$ sea state condition 2 occurring and with probability $p=0.2$ of sea state condition 3 occurring; same for current aligned with the direction of wind and waves and for the current opposing the wind and wave direction. The data is again presented for the 600 s and for 300 s simulation.



Graph 10 - Accumulated Damage over the three different current scenarios

The number of cycles allowed before structural failure is given based on Miner’s rule and presented in [Table 14](#).

Table 14 - Cycles to failure count

Scenario	Number of cycles to failure
No current	1.59E+11
Current aligned with wind	9.95E+11
Current opposite to wind	5.65E+10

5.2.Two blade HAWT

Results for static analysis were obtained for this WT option. The static analysis calculated the initial position of the system, which will be as described in Figure 21. These results are not useful for the FA of the system, as the time domain is not included in the calculations.

The dynamic analysis was run; however, no results were obtained, as a java specific error occurred. The .log file did not provide useful which would lead to resolution of the problem. The error message is provided in the [Figure 22](#). Data-check did not flag any invalid values in the task. Support from the software provider was requested, however, the support team was unfortunately not able to return to the error in time for the dissertation deadline.

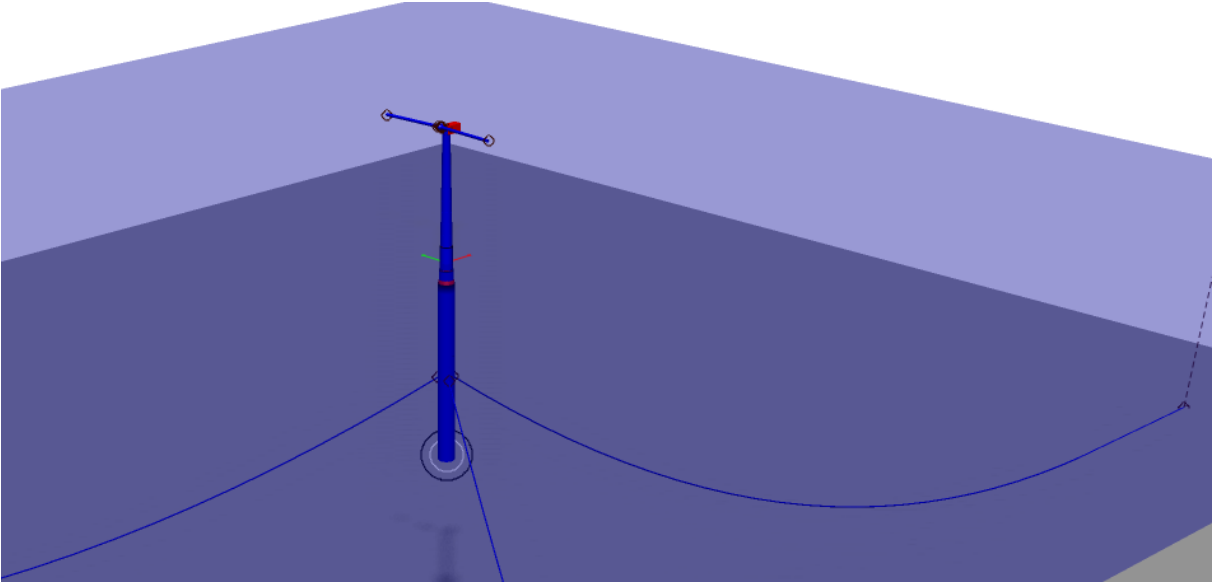


Figure 21 - Static position of the two blade HAWT

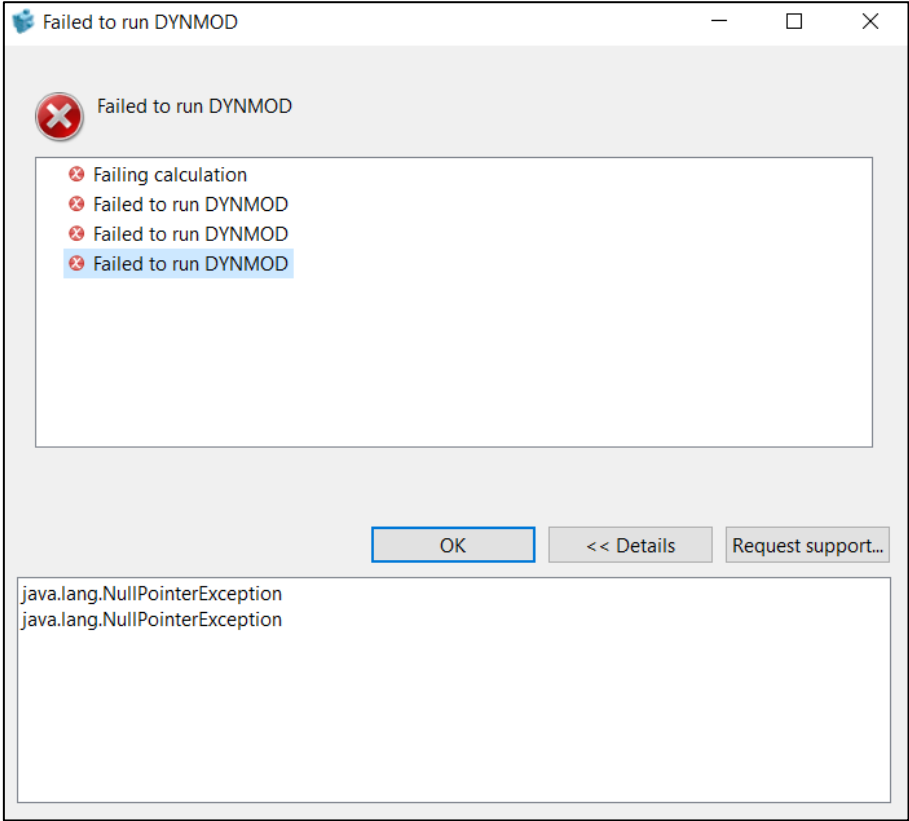


Figure 22 - Two blade HAWT dynamic calculation error message

5.3. VAWT

The vertical axis scenario proved to be the trickiest to model. The author was not able to obtain any results for this scenario due to the time limit. The model created had errors in itself and the author was not able to flat the errors. The error message is displayed in [Figure 23](#). The task does not display any errors when running the task check build-in feature of SIMA, however, the author suspects an error in the slender system connection between the turbine and the rest of the structure. The .log file does not provide sufficient information on the error either.

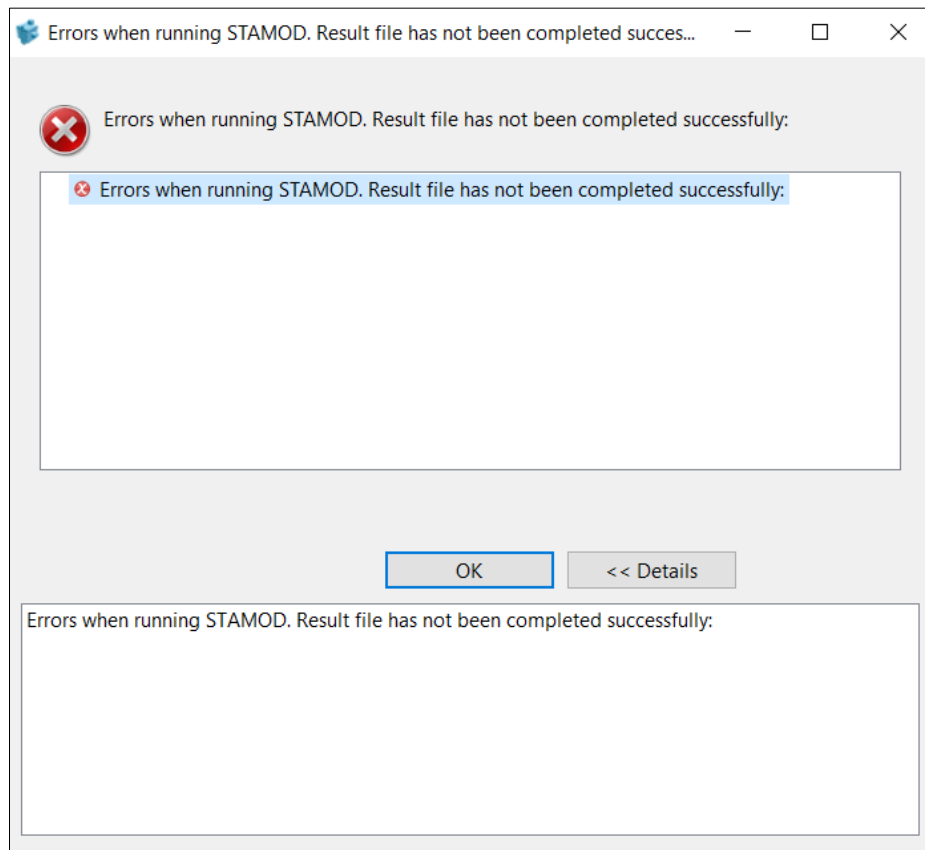


Figure 23 - VAWT task calculation error

6. Discussion

It was interesting to observe the fact that the wind turbine remained almost upright when the wind and wave came from one direction and the current was incoming from the opposite. The situation was created by the combination of the forces acting on the system. This may also be the reason why the 610 s simulation could not reach the end. As observed in [Figure 20\(c\)](#) the colour of the spar is different than in (a) and (b). The colour indicates the tension in the component. As the data of axial forces of the spar and mooring lines were not available due to the incomplete failing simulation, it may be argued the tension in the supporting structure was too high and lead to failure of the whole system respectively at simulation time $t_1=318$ s, $t_2=412$ s and $t_3=336$ s for sea state condition 1, 2 and 3 respectively.

Another thing to discuss is the result dependency on the simulation length. The same discussion is held in the R&D circles. The optimal time for a simulation length has not been agreed on yet. Comparing the results obtained from the two different simulation lengths it may be argued that for certain scenarios the shorter times of simulation are sufficient, in other cases it is not. The variable on which the time needed for a reliable simulation is vast. For example observed in the accumulated damage over the scenario with current aligned with the wind and wave direction, the results were not as different in both simulations ($error_2=17.65\%$) when compared to the scenario with no current ($error_1=61.31\%$) and current direction opposite to the wind and wave direction ($error_3=51.59\%$). In theory the simplest scenario had the biggest deviation between the two results. The $error_3$ is not representative, as the 600 s simulation was not successfully completed and the error would likely be greater.

At first the fatigue results seemed low, however, after considering the meaning of the data, and the part of the system under the consideration, the results seem reasonable. The damage calculated was per cycle (event), as presented in [Table 14](#), which considered the fact that offshore wind farms are designed for 20 operational years with the least maintenance possible, especially for a FOWT and the calculations on how many days within the specified condition simulated shows enough safety factor applied between the statistical occurrence of the sea state 6, sea state 7 and sea state 8 in the North Atlantic. It can be argued that in recent years the stormy sea conditions are occurring more often and that the number of days indicated in the long term statistical data due to the climate change. The long term data presented in 1982 states the probability of sea state 6 to occur is 18.7% of the year (68.26 days), the probability of occurrence of sea state 7 is 6.1% of the year (22.27 days) and of the sea state 8 it is 1.2% (4.38 days). Comparing these values to the data presented in the Table 14

which contains the number of events required the structure to fail. It should be emphasized that these values are for the modelled sea state conditions and do not account for other sea states and damaging events throughout the WT life.

To the surprise of the author great differences in damage were calculated. It was expected the stresses will vary greatly based on the sea state conditions, to the surprise, the data also varied based on the current. This would be expected for components such as the buoy and mooring system components, however, not to this extent in the case of the tower. The explanation is simple as the load transfer between the body parts. On the first thought one could assumed the bending moment and, therefore, the stresses would be greatest in the same wind + wave + current direction, as a result of a simple misconception of the model in our mind such as fixing the body in surge and sway at centre point at the WL, which is not corresponding to the reality. Same would be valid for the scenario with opposing current.

7. Conclusions

7.1. Conclusions

Based on the scope of this work, it may be concluded that the paper is not completely successful in comparing the different WT types like two blade HAWT and the VAWT models due to software failure and inability to solve the untraceable software errors or receive a response from the software developers due to time constraints. On the other hand the results obtained in general are interesting and potentially enhancing the robustness of the work done in the field of the HAWT research.

Based on the literature review it might have been favourable to make modifications the spar platform for the two blade HAWT. This could have been assumed based on the change of the weight and height of the system compared to the original WT for which the platform is intended for. This may lead to a conclusion that potential FA data obtained might have induced additional stresses to the tower compared to a manually designed support.

In the FA of a floating wind turbine it is important to include the loads from currents as it is recommended in the newest IEC WT standard series and demonstrated in Chen & Basu (2018). It is mainly important for fatigue calculations on the support and mooring as demonstrated in literature but differences in stresses and therefore fatigue damage are clear from the results also on the tower of the WT.

7.2. Lessons Learnt

Author recommends to the future researchers to familiarise themselves and install the software intended to be used as the first thing on their “to do” list. This is supported by the experience with OpenFAST code, which was intended to be used as major modelling tool for this work. The author neglected to check that and only rather late into the thesis writing process only realized the code does not run properly and no simulations can be run. It was more than challenging to learn how to operate a different piece of software within a month and a half time window. This was not managed by the author to an extent to execute the modelling task properly and therefore was unable to present all results, which is why the author feels that the work was not performed to the highest standard.

7.3. Future Work

Amongst suggestions to improvements to the models created and expanding the scenarios to different events as prescribed in the IEC 61400 standard line, it could be recommendable to feed a real data of environmental condition for a specific project location. As suggested before

a special spar should be designed for the two blade HAWT to make the results as accurate as possible.

The author also suggests developing the work further in the aspect of multi turbine interactions. The explore and compare the spacing between the WT in the VAWT and HAWT offshore wind parks and not only to see how the power extraction potential changes but as well investigate the changes in the fatigue predictions.

Special considerations for future work should be paid to the multi-turbine platforms and to multi-purpose platforms. The author recommends future work on comparison of fatigue on a multi-turbine platforms mounted with only with HAWT, only with VAWT and potentially with both WT concepts.

8. References

- Antonutti R. et al. (2016) “The effects of wind-induced inclination on the dynamics of semi-submersible floating wind turbine in the time domain” In: *Renewable Energy*, vol. 88 (2016), pp. 83-94
- Archer C. L., Jacobson M. Z. (2005), “Evaluation of global wind power”. In: *Journal of Geophysical Research*, vol. 110 (2005), pp. 1–20.
- Bales S. L. (1982) *Designing Ships to the Natural Environment*, Association of Scientists and Engineers of the Naval Sea Systems Command, Washington D. C.
- Borg M. et al. (2014), “Offshore floating vertical axis wind turbines, dynamics modelling state of the art. Part I: Aerodynamics”. In: *Renewable Energy and Sustainable Reviews*, vol. 39 (2014), pp. 1214-1225.
- Borg M. et al. (2014), “Offshore floating vertical axis wind turbines, dynamics modelling state of the art. Part II: Mooring line and structural dynamics”. In: *Renewable Energy and Sustainable Reviews*, vol. 39 (2014), pp. 122-1234.
- Borg M., Collu M. (2014), “Offshore floating vertical axis wind turbines, dynamics modelling state of the art. Part III: Aerodynamics”. In: *Renewable Energy and Sustainable Reviews*, vol. 46 (2015), pp. 296-310.
- BS EN IEC 61400-1:2019
- Burton T. et al. (2011), *Wind Energy Handbook*, West Sussex: J Willey & Sons, Ltd.
- Bussolari R. J. (not dated) *Status of the 4MW WTS-4 Wind Turbine*, Hamilton Standard Division of United Technologies, Windsor Locks
- Chen L., Basu B. (2018) “Fatigue load estimation of a spar-type floating offshore wind turbine considering wave-current interaction” In: *International Journal of Fatigue*, vol. 116 (2018), pp. 421-428

Cheng, Z.S. et al., (2017). “A comparison of extreme structural responses and fatigue damage of semi-submersible type floating horizontal and vertical axis wind turbines”. In: *Renewable Energy*, vol. 108, pp. 207-219.

Cradden L. et al. (2016) *The Offshore Environment*. In: Cruz J., Atcheson M. (eds) “*Floating Offshore Wind Energy. Green Energy and Technology.*” Springer, Cham.

Castro-Santos L., Diaz-Casas V. (eds) (2016) “*Floating Offshore Wind Farms. Green Energy and Technology.*” Springer, Cham.

Cruz J., Atcheson M. (eds) (2016) “*Floating Offshore Wind Energy. Green Energy and Technology.*” Springer, Cham.

Dinh V.N., & Basu B. (2013). *On the Modeling of Spar-type Floating Offshore Wind Turbines*.

DNV-GL (2017), DNVGL-RP-C205, *Environmental conditions and environmental loads*

Energy Technologies Institute (2015), *Offshore Wind Floating Wind Technology Key Headlines*

Hand B., Cashman A. (2017) “Conceptual design of large-scale floating offshore vertical axis wind turbine” In: *Energy Procedia*, vol: 142 (2017), pp. -83-88,

Hansen J., et al. (1980), “Climate impact of increasing atmospheric carbon dioxide”. In: *Science*, 213 (1980), pp. 957-966

Hardy, Chris (6 July 2010). ["Renewable energy and role of Marykirk's James Blyth". *The Courier*. Dundee: D. C. Thomson & Co. Archived from *the original* on 10 July 2010. Retrieved 12 December 2010](#)

Hau E. (2013) *Wind turbines: fundamentals, technologies, application, economics*; 3rd edn. Springer-Verlag, Berlin, Heidelberg

Henderson A., et al. (2016) Overview of Floating Offshore Wind Technologies. In: Cruz J., Atcheson M. (eds) *“Floating Offshore Wind Energy. Green Energy and Technology.”* Springer, Cham.

Islam M. et al. (2013,) “Progress and recent trends of wind energy technology”. In: *Renewable and Sustainable Energy Reviews* vol. 21 (2013), pp. 456–68.

Jacobson M. Z. (2016), “Clean grids with current technology”. In: *Nature Climate Change*, vol. 1 (2016), pp. 1-2, 10.1017/CBO9781107415324.004.

Jason M. et al. (2005) *FAST User’s Guide*, NREL

De Jonge J. B. (1970) “The Monitoring of Fatigue Loads” In: *The Seventh Congress of the International Council of the Aeronautical Sciences*”, Rome, Italy 1970

Jonkman J.M., (2007). *Dynamics Modeling and Loads Analysis of an Offshore Floating Wind Turbine*. University of Colorado at Boulder.

Jonkman J. M., Buhl Jr. M. L. (2007), “Development and verification of a fully coupled simulator for offshore wind turbines,” in 45th AIAA Aerospace Sciences Meeting and Exhibit, Reno, Nevada, 2007, pp. 28–53.

Jonkman J. M. et al. (2009), “Definition of a 5-MW Reference Wind Turbine for Offshore System Development”, NREL

Jonkman J. M. (2010) “Definition of the Floating System for Phase IV of OC3”, NREL

Lee, Yung-Li et al. (2011) “Metal Fatigue Analysis Handbook: Practical Problem-solving Techniques for Computer-aided Engineering”, Butterworth Heinemann

Available at: <https://www.dawsonera.com:443/abstract/9780123852052>

Li H. et al. (2017) “Short –term fatigue analysis for tower base of a spar-type wind turbine under stochastic win-wave loads” In: *International Journal of Naval Architecture and Ocean Engineering*, vol. XX (2017), pp. 1-12

Li L. et al. (2019) *Ultimate structural fatigue damage loads of a spar-type floating wind turbine*, University of Strathclyde

Ma K.-T., Luo Y., Kwan T., Wu Y. (2019) “*Mooring System Engineering for Offshore Structures*”, Gulf Professional Publishing, ISBN 9780128185513, <https://doi.org/10.1016/B978-0-12-818551-3.00002-8>.

Ma Y. et al. (2013) “Wind-wave induced dynamic responses analysis for motions and mooring loads of a spar type offshore floating wind turbine” In: *Journal of Hydrodynamic*, vol. 26, (2014), pp. 865-874.

Matha D. et al. (2016) Modelling of Floating Offshore Wind Technologies. In: Cruz J., Atcheson M. (eds) “*Floating Offshore Wind Energy. Green Energy and Technology.*” Springer, Cham.

Merz K. O. (2012), “A Method for Analysis of VAWT Aerodynamic Loads under Turbulent Wind and Platform Motion” In: *Energy Procedia*, vol. 24 (2012), pp. 44-51.

Moore A. et al. (2018) “The role of floating offshore wind in a renewable focused electricity system for Great Britain in 2050” In: *Energy Strategy Reviews*, vol. 22 (2018), pp. 270-278.

Munk WH (1950) Origin and generation of waves. In: *Proceedings of the 1st international conference on coastal engineering*, long beach, California. ASCE, pp 1–4.

Neill S. P., Hashemi M. R. (2018), *Fundamentals of Ocean Renewable Energy - Generating Electricity from the Sea*, Elsevier Ltd, London

PD IEC TS 61400-3-2:2019

Robertson A. N., Jonkman J. M. (2011) *Loads Analysis of Several Offshore Floating Wind Turbine Concepts*, International Society of Offshore and Polar Engineers 2011 Conference

Santos-Alamillos F.J., et al., (2014), A methodology for evaluating the spatial variability of wind energy resources: Application to assess the potential contribution of wind energy to baseload power: *Renew. Energy*, vol. 69 (2014), pp. 147-156.

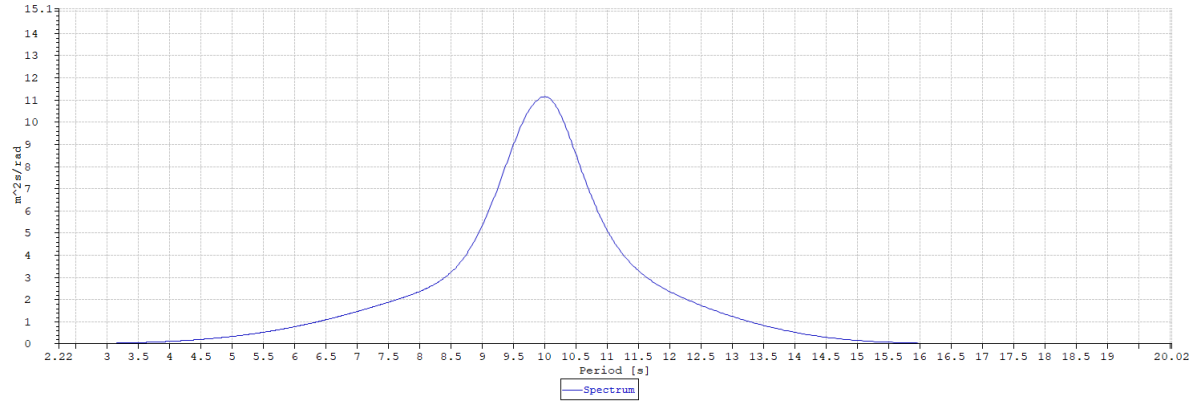
- Schweigler, K., 2012. *Aerodynamic Analysis of the NREL 5-MW Wind Turbine Using Vortex Panel Method*, Gothenburg: Chalmers University of Technology.
- Susmel L., Lazzarin P. (2001) *A bi-parametric Wöhler curve of high cycle multiaxial fatigue assessment*, University of Padova
- Sutherland H. J. (1999), “*On the Fatigue Analysis of Wind Turbines*”, Sandia National Laboratories, New Mexico
- Tupper E. C. (2013), *Introduction to Naval Architecture* (Fifth Edition), Butterworth-
- Vita L. (2011) *Offshore Vertical Axis Wind Turbine with Floating and Rotating Foundation*, DTU
- Whittlesey R. W. et al. (2010) “Fish schooling as a basis for vertical axis wind turbine farm design.” In: *Bioinspiration and Biomimetics* 5(no.3).
- WindEurope (February 2019) “*Offshore Wind in Europe – Key trends and statistics 2018*”
<https://www.theclimatemobilization.org/> Accessed on: 29. 06. 2019
- World Meteorological Organization (2014, updated 2017) *Guide to meteorological instruments and methods of observation*, 8th edn. WMO-No. 8, Geneva, Switzerland
- Wu X. et al. (2019) “Foundations of offshore wind turbines: A review” In: *Renewable and Sustainable Energy Reviews*, vol. 104 (2019), pp. 379-393

Appendix 1

The wave spectrum for the basic scenario

Direction	Spreading Type	Spreading Exponent	Number of Directions	Significant Wave Height	Peak Period	Gamma
0.0	Unidirectional	2.0	11	6.0	10.0	3.3

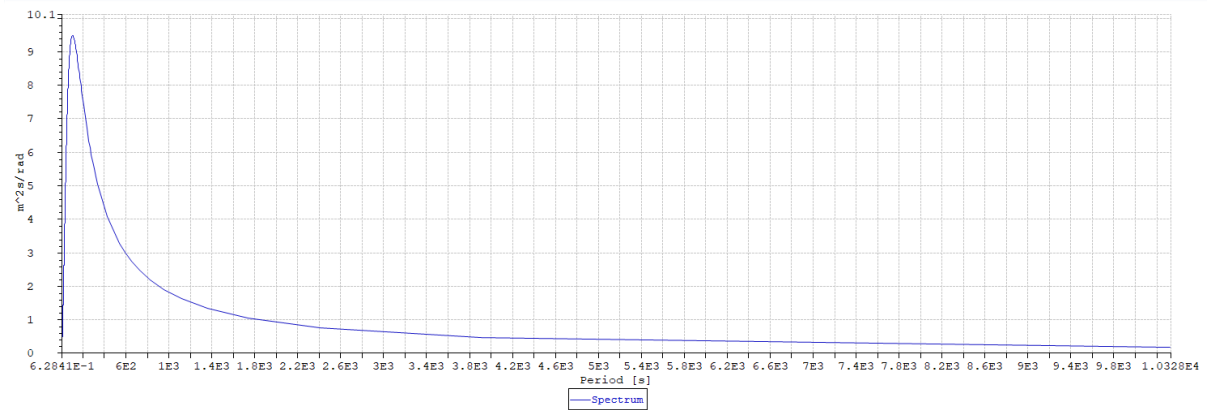
Wave spectrum



The wind spectrum

Direction	Profile Exponent	Average Velocity	Friction	Reference Height	Reference Length
0.0	default	15.0	default	default	default

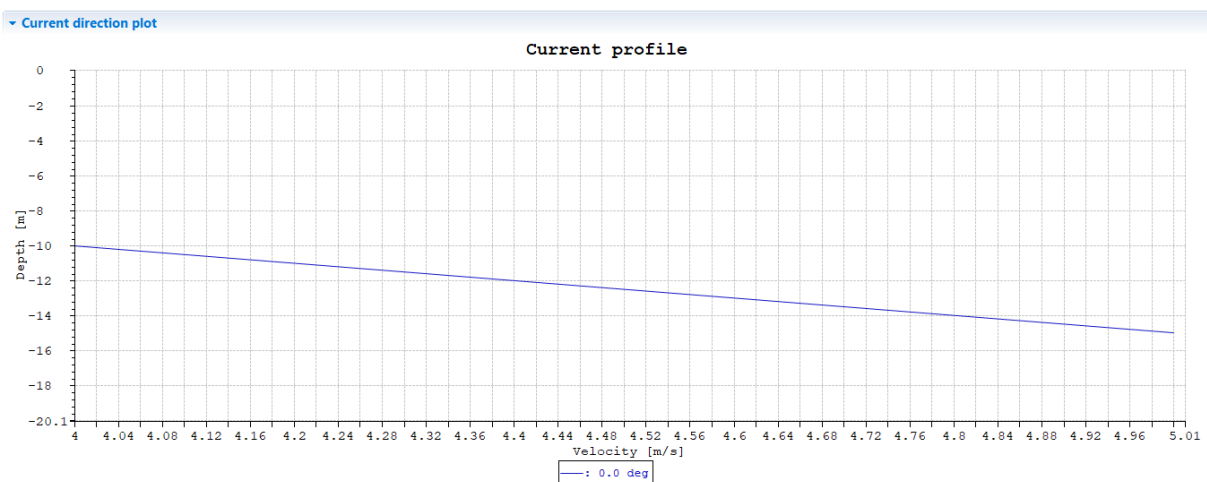
Wind spectrum



The current profile

No	Level	Direction	Velocity
1	-10.0	0.0	4.0
2	-15.0	0.0	5.0

Current direction plot



Appendix 2

Hydrostatic Stiffness Matrix of the spar for VAWT

	Surge	Sway	Heave	Roll	Pitch	Yaw
Surge	0.000E+00	0.000E+00	0.000E+00	0.000E+00	0.000E+00	0.000E+00
Sway	0.000E+00	0.000E+00	0.000E+00	0.000E+00	0.000E+00	0.000E+00
Heave	0.000E+00	0.000E+00	3.082E+05	1.458E+01	-4.786E+02	0.000E+00
Roll	0.000E+00	0.000E+00	1.458E+01	1.039E+09	1.611E+00	1.547E+01
Pitch	0.000E+00	0.000E+00	-4.786E+02	1.611E+00	1.039E+09	-2.648E+03
Yaw	0.000E+00	0.000E+00	0.000E+00	0.000E+00	0.000E+00	0.000E+00

Hydrostatic Stiffness of the spar for HAWT

	Surge	Sway	Heave	Roll	Pitch	Yaw
Surge	0.000E+00	0.000E+00	0.000E+00	0.000E+00	0.000E+00	0.000E+00
Sway	0.000E+00	0.000E+00	0.000E+00	0.000E+00	0.000E+00	0.000E+00
Heave	0.000E+00	0.000E+00	3.337E+05	0.000E+00	0.000E+00	0.000E+00
Roll	0.000E+00	0.000E+00	0.000E+00	1.590E+09	0.000E+00	0.000E+00
Pitch	0.000E+00	0.000E+00	0.000E+00	0.000E+00	1.590E+09	0.000E+00
Yaw	0.000E+00	0.000E+00	0.000E+00	0.000E+00	0.000E+00	9.834E+07

Potential Damping Matrix at infinite frequency of the the Spar for VAWT

	Surge	Sway	Heave	Roll	Pitch	Yaw
Surge	2.608E-01	-1.431E-04	-2.945E-05	-4.613E-03	-1.579E+01	2.241E-06
Sway	2.129E-04	2.607E-01	1.071E-04	1.578E+01	-1.098E-02	-3.390E-07
Heave	5.935E-05	-4.470E-05	-2.570E-04	-2.727E-03	-3.900E-03	-1.385E-07
Roll	2.474E-03	1.623E+01	3.985E-03	9.823E+02	-8.450E-02	-2.094E-05
Pitch	-1.624E+01	4.243E-03	1.719E-03	4.513E-02	9.828E+02	-1.362E-04

Yaw 4.830E-06 9.298E-06 1.522E-07 5.744E-04 -3.111E-04 1.842E-09

Damping of the OC3 Spar

	Surge	Sway	Heave	Roll	Pitch	Yaw
Surge	1.000E+05	0.000E+00	0.000E+00	0.000E+00	0.000E+00	0.000E+00
Sway	0.000E+00	1.000E+05	0.000E+00	0.000E+00	0.000E+00	0.000E+00
Heave	0.000E+00	0.000E+00	1.300E+05	0.000E+00	0.000E+00	0.000E+00
Roll	0.000E+00	0.000E+00	0.000E+00	0.000E+00	0.000E+00	0.000E+00
Pitch	0.000E+00	0.000E+00	0.000E+00	0.000E+00	0.000E+00	0.000E+00
Yaw	0.000E+00	0.000E+00	0.000E+00	0.000E+00	0.000E+00	1.300E+07

Appendix 3

Tables of cross-sections defined for the two blade HAWT

▼ Generic Axisymmetric Pipe

Name	Cross section type	Mass coeff.	Ext. Area	Int. Area
shaft1	Beam	4660.0	7.06	0.0
shaft2	Beam	100.0	7.06	0.0
ecc	Beam	100.0	0.01	0.0
tower1	Beam	4506.1	30.5	0.0
tower2	Beam	4190.0	28.03	0.0
tower3	Beam	3885.2	25.62	0.0
tower4	Beam	3591.4	23.31	0.0
tower5	Beam	3308.9	21.11	0.0
tower6	Beam	3037.6	19.03	0.0
tower7	Beam	2777.4	17.05	0.0
tower8	Beam	2528.5	15.18	0.0
tower9	Beam	2290.8	13.42	0.0
tower10	Beam	2064.3	11.76	0.0
mo_wire	Bar	77.707	0.0063617	0.0
dummy	Beam	0.0	0.0	0.0

▼ Double Symmetric Cross Section

Name	Cross section type	Mass coeff.	Ext. Area	Int. Area
foil_01	Beam	802.72	1.0	0.0
foil_02	Beam	634.78	1.0	0.0
foil_03	Beam	427.78	1.0	0.0
foil_04	Beam	445.16	1.0	0.0
foil_05	Beam	368.3	1.0	0.0
foil_06	Beam	353.51	1.0	0.0
foil_07	Beam	335.1	1.0	0.0
foil_08	Beam	306.31	1.0	0.0
foil_09	Beam	272.38	1.0	0.0
foil_10	Beam	245.49	1.0	0.0
foil_11	Beam	201.2	1.0	0.0
foil_12	Beam	167.84	1.0	0.0
foil_13	Beam	140.58	1.0	0.0
foil_14	Beam	107.47	1.0	0.0
foil_15	Beam	90.807	1.0	0.0
foil_16	Beam	70.843	1.0	0.0
foil_17	Beam	48.356	1.0	0.0

Table of nods defined for two blade HAWT

Name	Constraint	X G Initial	Y G Initial	Z G Initial	Reference Frame
anchor_1	Fixed or Prescribed	907.4	0.0	-70.0	- GLOBAL -
anchor_2	Fixed or Prescribed	-453.7	785.83	-70.0	- GLOBAL -
anchor_3	Fixed or Prescribed	-453.7	-785.83	-70.0	- GLOBAL -
tp_1	Slaved	5.2	0.0	-70.0	- GLOBAL -
tp_2	Slaved	-2.6	4.5	-70.0	- GLOBAL -
tp_3	Slaved	-2.6	-4.5	-70.0	- GLOBAL -
sparloc	Free	0.0	0.0	0.0	- GLOBAL -
towerlow	Slaved	0.0	0.0	10.0	- GLOBAL -
towerup	Free	0.0	0.0	87.6	- GLOBAL -
sh_sn1	Free	-5.0	0.0	90.0	- GLOBAL -
sh_sn2	Slaved	-4.0038	0.0	89.913	- GLOBAL -
bl1e_sn2	Free	-5.0652	1.4986	90.006	- GLOBAL -
bl1f_sn1	Slaved	-5.0652	1.4986	90.006	- GLOBAL -
bl1f_sn2	Free	-7.7376	62.94	90.24	- GLOBAL -
bl2e_sn2	Free	-5.0652	-1.4986	90.006	- GLOBAL -
bl2f_sn1	Slaved	-5.0652	-1.4986	90.006	- GLOBAL -
bl2f_sn2	Free	-7.7376	-62.94	90.24	- GLOBAL -